Chapter 3

Dual-receptor targeted chitosan nanoparticles of docetaxel

3. Dual-receptor targeted chitosan nanoparticles of docetaxel (DXL)

3.1 Objective

The objective of this study to prepare DXL loaded, dual receptor (folate and EGFR) targeted chitosan nanoparticles (CS-NPs) and characterized their physicochemical properties such as shape, particle size, zeta-potential. surface morphology and surface chemistry, *in-vitro*, cytotoxicity against A-549 cells, *in-vivo* pharmacokinetic, histopathology and *in-vivo* anticancer efficacy in B(a)P induced lung cancer mice.

3.2 Plan of study

1. Preparation and characterization of chitosan-folate conjugate
2. Preparation and characterization of TPGS-COOH
3. Preparation of DTX loaded dual receptor targeted CS-NPs using solvent evaporation combined with ionic cross-linking method.
4. Physicochemical and *in-vitro* evaluation of dual-receptor targeted CS-NPs
   - Particle size, polydispersity index and zeta potential
   - Electron microscopy (SEM, TEM & AFM)
   - Crystallographic studies by XRD
   - Surface chemistry by XPS
   - Determination of entrapment efficiency
   - *In-vitro* drug release studies
   - *In-vitro* cellular uptake study on A-549 cells
   - *In-vitro* cytotoxicity on A-549 and SIRC cells

5. *In-vivo* evaluation of dual receptor targeted CS-NPs
   - Pharmacokinetic studies in Wistar rats
   - Histopathology studies in Wistar rats
   - Anticancer efficacy studies on B(a)P induced lung cancer mice model

3.3. Material

Docetaxel (99.56% pure) was a kind gift by Neon Laboratories Ltd, Mumbai India. 1-Ethyl-3-(3-dimethylaminopropyl) carbodiimide (EDC) and high molecular weight chitosan (MW~30 kDa, based on viscosity, degree of deacetylation ≥ 90%) were bought from Sisco Research Laboratory Pvt. Ltd. D-alpha-tocopheryl-polyethyleneglycol-1000-succinate (TPGS) was provided as a gift sample by PMC Isochem, France. Folic acid was procured from Loba Chemie, Pvt. Ltd., Mumbai, India. Sodium TPP, cetuximab, coumarin 6 (C6), penicillin and streptomycin and N-hydroxy succinimide (NHS) were obtained from Sigma-Aldrich, St. Louis, MO, USA. Dialysis membrane (Spectra/Por7®) of molecular weight 1 KDa was bought from Spectrum Laboratories Inc., Rancho Dominguez, CA, U.S.A. A-549 lung cancer cell line was provided by the National Centre for Cell Science (NCCS), Pune, India. Dulbecco's modified Eagle's medium (DMEM), 3-(4,5-dimethyl thiazolyl-2-yl)-2,5-diphenyltetrazolium bromide (MTT) and trypsin-EDTA were bought from Thermo Fisher Scientific, Mumbai, India. Dimethyl sulfoxide and ethanol were obtained from Merk, Darmstadt, Germany. L-glutamine and fetal bovine serum (FBS) were bought from Genetix Biotech Asia Pvt. Ltd., Mumbai, India. All other chemicals and reagents utilized were pure and of analytical grade.

3.4. Methods

3.4.1. Synthesis of chitosan-folate (CS-F) conjugate

The CS-F conjugate was synthesized by carbodiimide chemistry with slight modification of methods reported previously [168]. Briefly, 44 mg of folic acid and 76 mg of 1-(3-dimethyl aminopropyl)-3-ethyl carbodiimide hydrochloride (EDC) were solubilized in 15 mL of anhydrous dimethyl sulfoxide (DMSO) and stirred for 1 h at room temperature. Chitosan solution (0.6%) was prepared by dissolving 153 mg of chitosan in acetate buffer

(pH 4.7) and mixed it to the folic acid solution, followed by stirring in the dark for 16 h. Afterwards, the pH of the above solution was brought to 9.0 with aqueous NaOH. The resulting solution was dialyzed against Phosphate buffer saline (PBS) (pH 7.4) for 3 days using 1KDa dialysis membrane and then in distilled water for the following 3 days. The resultant dark brownish precipitate was subjected to freeze-drying for up to 24 h to get a dry powder [169]. The synthesis of CS-F is depicted in **Figure 3.1**.

3.4.2. Characterization of CS-F

To characterize the synthesized CS-F conjugate, various spectroscopic methods were used, including ^{1}H-NMR spectroscopy (One Bay NMR Spectrometer; Bruker Biospin International), Fourier-transform infrared spectroscopy (FTIR) (ATR, Thermo Electron Scientific Instruments LLC) and Mass spectroscopy (TOF-MS).

3.4.2.1. Degree of folic acid substitution

The degree of the folic acid substitution to the chitosan (CS) was determined by using a multi-mode microplate reader (Molecular Devices, USA). Concisely, 2 mg of the CS-F conjugate was vortexed in 10 mL mixture of dimethyl sulfoxide (DMSO) and dichloromethane (DCM) (4:1) for 6 h. After centrifugation, the samples were filtered, and the supernatant was examined for UV analysis after the desired dilution. The folate content was calculated by plotting the folic acid calibration curve at λ max of 363 nm, and the degree of folic acid substitution was determined by the given formula [170,171].

$$Degree\ of\ folic\ acid\ sustitution\ (\%) = \frac{F/MW_{FA}}{(CSF - F) * MW_{CS}} \times 100$$

Where F is the folic acid content determined by UV analysis; MW_{FA} is the molecular weight of the folic acid, CSF is the total amount of the chitosan-folate taken, and MW_{CS} is the molecular weight of the single unit of the CS.

3.4.3. Preparation of TPGS- COOH

TPGS-COOH was prepared through ring opening reaction of the succinic anhydride in the presence of the DMAP. Briefly, 0.5 mmol of TPGS (0.77 g), 1 mmol of succinic anhydride (0.10 g) and 1 mmol of DMAP (0.12 g) were mixed and stirred for 24 h at 100 °C under N_2 atmosphere. The hot solution was then allowed to come down to ambient temperature. Following, 5 mL ice-cold DCM was added to the above solution. Unreacted succinic anhydride was separated by filtration. Diethyl ether (100 mL) was then added to the above solution at -10 °C and kept overnight for precipitation. The white TPGS-COOH precipitate was collected by filtration and dried under vacuum [172,173].

3.4.4. Characterization of TPGS-COOH

Synthesized TPGS-COOH was characterized by FTIR, NMR and Mass spectroscopy. The dried sample was used for the FTIR analysis, whereas deprotonated DMSO was used as the solvent for NMR spectroscopy. For mass spectroscopy, the dried sample was dissolved in deionized water [162].

3.4.5. Preparation of DXL/C6 loaded dual EGFR and folate-targeted nanoparticles

All chitosan nanoparticles (CS-NPs) were prepared by a previously reported method with some modifications [174]. In brief, required quantities of chitosan and chitosan-folate, as specified in table 1, were dissolved in the aqueous acetic acid solution (0.2% v/v). The pH of the above solution was adjusted to 6.0 using aqueous NaOH. 1 mL of TPGS/TPGS-COOH solution (20 mg/mL) was then added to the above solution. DXL (3 mg) or C6 (0.3 mg) was dissolved in 1 mL chloroform and mixed with chitosan solution and using an ultrasonic probe sonicator (Hielscher UP200H, Germany), the mixture was sonicated for 5 min in an ice bath which made it milky white (micro-emulsion). The above emulsion was kept for stirring overnight which is required for the complete evaporation of

chloroform. Further cross-linking was achieved by slowly adding 2.5 mL of 2 mg/mL solution of sodium tripolyphosphate (Na-TPP) dropwise and then stirred for 1 h. To bring about surface conjugation, EDC: NHS in the molar ratio of 1:5 were added to the above solution and stirred for 30 min. Following, 2.5 mg of cetuximab was added and continuously stirred for 30 min. The resulting nanoparticle suspension was dialyzed against the saturated solution of DXL using a 1 KDa dialysis membrane. To separate larger particles, all nanoparticle formulations were centrifuged for 10 min at 1000 rpm and then filtered through a 0.22 µm membrane filter.

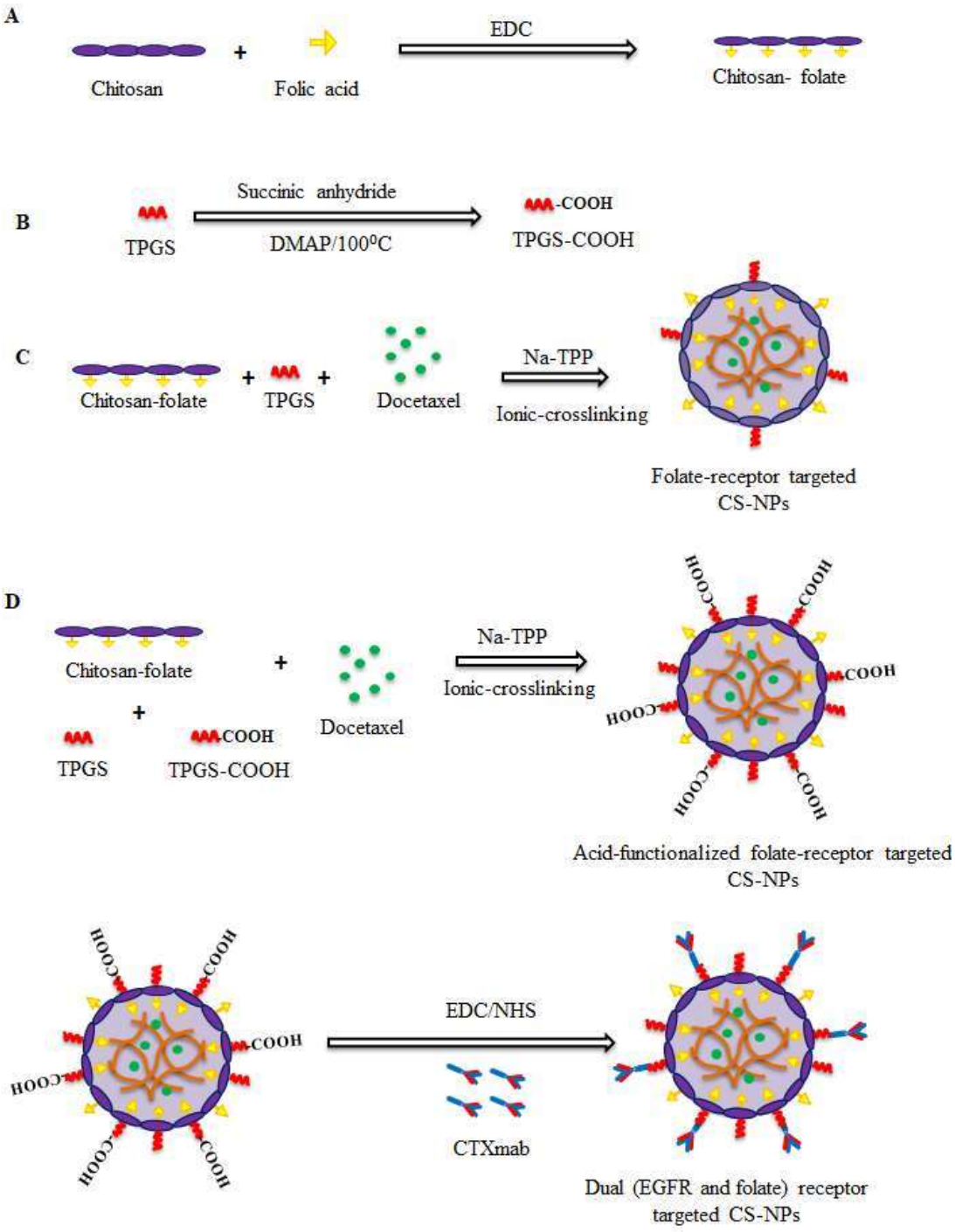

Figure 3.1. Schematic diagram for the synthesis of A) chitosan-folate, B) TPGS-COOH, C) folate-receptor targeted CS-NPs, D) dual-receptor targeted CS-NPs

3.4.6. Nanoparticles characterization

3.4.6.1. Particle size, polydispersity and surface charge

Particle size, polydispersity and surface charge of nanoformulations were analyzed by dynamic light scattering technique (Malvern Zetasizer Nanoseries) at 25 °C. The values reported are the average of three runs performed for each sample [175].

Table 3.1. Formula of various CS-NPs

Batches	Chitosan-Folate (mg)	Chitosan (mg)	TPGS (mg)	TPGS-COOH (mg)	DXL (mg)	C6 (mg)	Sodium TPP (2 mg/ml)
DXL- CS-NPs	0	30	20	-	3	-	2.5
DXL-CS-F-NPs	9	21	20	-	3	-	2.5
DXL-CS-CTXmab-NPs	0	30	10	10	3	-	2.5
DXL-CS-F-CTXmab-NPs	9	21	10	10	3	-	2.5
C6- CS-NPs	0	30	20	-		0.3	2.5
C6- CS-F-NPs	9	21	20	-		0.3	2.5
C6- CS-CTXmab-NPs	0	30	10	10		0.3	2.5
C6- CS- F-CTXmab - NPs	9	21	10	10		0.3	2.5

DXL-CS-NPs: DXL loaded CS-NPs
DXL-CS-F-NPs: DXL loaded folate-receptor targeted CS-NPs
DXL-CS-CTXmab-NPs: DXL loaded EGFR targeted CS-NPs
DXL-CS-CTXmab-F-NPs: DXL loaded dual-receptor targeted CS-NPs
C6- CS-NPs: C6 entrapped chitosan NPs
C6- CS-F-NPs: C6 entrapped folate-receptor targeted CS-NPs
C6- CS-CTXmab-NPs: C6 entrapped EGFR targeted CS-NPs
C6- CS-CTXmab-F-NPs: C6 loaded dual-receptor targeted CS-NPs

3.4.6.2. Transmission electron microscopy (TEM) analysis

The shape, size and morphology of CS-NPs were characterized by transmission electron microscopy (Philips CM-12., Fullerton, CA). All nanoparticle formulations were diluted (five times in purified water) and sonicated for 2 min. One drop from each diluted sample was placed on the TEM grids, dried under vacuum overnight, and then subjected to TEM analysis [176].

3.4.6.3. Scanning electron microscopy (SEM) analysis

Surface morphology of CS-NPs was observed by scanning electron microscope (MA15/18, Carl Zeiss Microscopy Ltd). Images were taken at 50 KX magnification and at 20 kV. All the samples were diluted up to five times with ultrapure water and one drop from each of the diluted samples was put on the coverslips followed by the drying for 24 h in a hot air oven at 40 °C. Respective slides were processed with carbon coating and subjected to the SEM analysis [177].

3.4.6.4. Atomic force microscopy (AFM) analysis

AFM analysis of CS-NPs at the nanoscale was carried out by using NTEGRA Prima AFM (NT-MDT Service & Logistics Ltd.). Nanoparticle suspension was diluted up to five times and sonicated for 10 min. The samples were prepared by putting a drop of nanoparticle formulation on a glass slide (2 x 2 cm) and vacuum drying for 24 h (film formation) was done. 2-D and 3-D AFM images of nanoparticles were then [178].

3.4.6.5. X-ray photoelectron spectroscopy (XPS) analysis

The surface chemistry of CS-NPs was analyzed by X-ray photoelectron spectroscopy (K-Alpha, Thermo Fisher Scientific) at the binding energy of 100-700 eV. Samples were prepared by putting a drop of nanoparticle suspension on a glass slide and dried overnight under a vacuum dryer [179,180].

3.4.6.6. Degree of conjugation

3.4.6.6.1. Folic acid content

The folate content in DXL-CS-F-NPs and DXL-CS-F-CTXmab-NPs was determined by using a multi-mode microplate reader (Molecular Devices, USA). Concisely, 200 µL of the nanoparticles were freeze-dried and dissolved in the DMSO: DCM (4:1). After vortexing for 6 h, samples were centrifuged, and the filtered supernatant was used for the

UV-Visible analysis. The calibration curve of the folic acid at λ max = 364 nm was prepared, and the total folic acid content present in the folate conjugated CSA-NPs was determined. The percent folic acid content was computed by the given formula [171].

$$Degree\ of\ folate\ conjugation\ (\%) = \frac{Folate\ content\ determined\ within\ NPs}{Total\ folate\ content\ used\ in\ NPs} * 100$$

3.4.6.6.2. CTXmab content

The extent of cetuximab conjugation in the single EGFR targeted and dual folate and EGFR targeted NPs was evaluated by Bradford [179]. For this, 1ml of each of the above NPs and blank PBS pH 7.4 and standard cetuximab solution were made to react for 5 min with 5 ml Bradford reagent separately and the respective UV absorbances were recorded. The total amount of cetuximab conjugated onto the targeted NPs was then derived from the calibration curve of bovine serum albumin (BSA).

$$Degree\ of\ CTXmab\ conjugation\ (\%) = \frac{CTXmab\ content\ determined\ in\ NPs}{CTXmab\ content\ in\ std.\ solution} * 100$$

3.4.6.7. Entrapment efficiency

The entrapment efficiency of CS-NPs was determined by HPLC analysis (Shimadzu 1800, Tokyo, Japan). Concisely, 200 µL (~60 µg of DXL) of the nanoparticle suspension was transferred to a round bottom flask and subjected to evaporation. Acetonitrile/ methanol/ water system in the ratio 40/5/55 was used as mobile phase for HPLC. Dried content was dissolved in 100 µL of mobile phase and vortexed for 15 min. Then, centrifugation of all the samples for a period of 15 min was carried out at 10,000 rpm. 100 µL from the supernatant was added to the HPLC vials. The standard curve of DXL was obtained in methanol and the same was utilized to compute the DXL concentrations

of above samples by using HPLC. The graph was plotted between concentrations (10-10,000 ng) against peak area which appeared almost linear curve with regression coefficient R^2 = 0.998. The percent drug entrapped in nanoparticle formulations was computed from the ratio of quantity of DXL loaded to the actual amount of DXL added during method of preparation. The entrapment efficiency of C6 loaded formulations was measured by fluorescence spectroscopy. Briefly, 30 µL of nanoparticle suspension was taken and evaporated by a rotary evaporator. Dried C6 content was then dissolved in 70 µL of methanol which was further mixed with distilled water up to 1 mL and filtered with 0.22 µm syringe filter. The excitation (462 nm) and emission (502 nm) wavelengths in the fluorometer were adjusted. The percent C6 entrapped in nanoparticle formulations was calculated using the same formula [181].

3.4.6.8. X-ray diffraction (XRD) analysis

XRD analysis of DXL, DXL-CS-NPs, DXL-CS-F-NPs, DXL-CS-CTXmab-NPs and DXL-CS-CTXmab-NPs was performed by using Bench Top X-Ray Diffraction (BT-XRD: RIGAKU Corporation). The DXL was used in powder form while all the DXL loaded CS nanoparticles were lyophilized for 12 h prior to the XRD analysis [182].

3.4.7. In-vitro evaluation

3.4.7.1. In-vitro release study

The drug release profile of DXL from prepared nanoformulations was determined by the dialysis bag diffusion method. An equivalent volume, of the respective nanoparticles, to 0.3 mg of DXL was kept in a dialysis bag (1 KDa) and sealed hermetically. This dialysis bag was immersed into a beaker containing 50 mL medium (PBS, pH 7.4 and pH 5.5). The total setup was placed in a water bath shaker (REMI CM-12 Plus, Mumbai, India) at 37 ± 0.5 °C with continuous shaking. As per the predetermined time schedule, 1 mL

samples were taken and the same volume was replenished with a fresh medium. Before analysis, filtration through a 0.22 µm syringe filter was done for all samples and for the extraction of docetaxel, 1ml of ethyl acetate was added. The ethyl acetate was separated from all the samples after vortexing and allowed to evaporate for complete dryness. The dry residue containing docetaxel was then dissolved in the 90 µL of mobile phase (acetonitrile, methanol and water in the ratio 45: 45: 10) and analyzed by HPLC (triplicate). A graph of cumulative drug release against time was plotted [183].

3.4.7.2. In-vitro cellular uptake study

The extent of cellular uptake of C6 loaded formulations (C6-CS-NPs, C6-CS-F-NPs, C6-CS-CTXmab-NPs and C6-CS-CTXmab-F-NPs) was evaluated on A-549 cells using a fluorescence microscope. At the density of $5x10^4$ cells per well, cells were seeded in 12-well plates and incubated for 24 h. Following, free C6 and C6 loaded formulations were added to the wells at 5 µg/mL concentration in the complete DMEM and incubated for 1 h at 37 ℃. The cells were then fixed for 15 min with a 4% formaldehyde solution after being rinsed three times with PBS. Further, cells were treated with 4′,6-diamidino-2-phenylindole (DAPI) for the staining of the nuclei. The medium containing DAPI was removed from the wells after 15 min and the cells were again irrigated with PBS. Fluorescence images of internalized nanoparticles were observed in a comparable blue channel (DAPI) and green channel (C6) at excitation wavelengths of 340 nm and 488 nm respectively. The extent of cellular uptake of C6 loaded nanoparticles was quantified using image-J software. The percent area of green channels was observed, which indicated the internalization of nanoparticles in A-549 cells [184].

3.4.7.3. In-vitro cytotoxicity study

In-vitro cytotoxicity of DXL-CS-NPs, DXL-CS-F-NPs, DXL-CS-CTXmab-NPs, DXL-CS-F-CTXmab-NPs was assessed in comparison to DXL control by performing MTT assay on A-549 and SIRC cells. The cells were seeded into 96-well plates at the density of 5×10^4 viable cells/well in DMEM and incubated at 37 ºC for 24 h in CO_2 humidified incubator (5%) to permit proper cell attachment. Subsequently, the depleted media was discarded and the cells were treated with respective nanoparticle formulations in DMEM at the equivalent concentrations from 0.025 to 25 µg/mL (triplicate) for 24 h. Afterward, media containing treatments were discarded and 90 µL of fresh medium along with 10 µL of MTT solution (5 mg/mL in PBS, pH 7.4) were instilled into treated wells. Incubation of the plates, again for 4 h, was carried out. Consequently, the resulting MTT-formazan crystals were isolated by removing the medium carefully without disturbing the crystals and then dissolved by the addition of 100 µL of DMSO. The absorbance was read at 570 nm by a microplate reader and the percent cell viability was calculated as the percentage of treated cells in comparison to untreated cells [185]. The percent cell viability was computed by using the formula below:

$$\text{Cell viability (\%)} = \frac{\text{Absorbance of treated cells}}{\text{Absorbance of control cells}} \text{ X } 100$$

3.4.8. In-vivo characterization

3.4.8.1. Pharmacokinetic study

Healthy Wistar rats of 4-5 weeks age and weighing about 150–200 g were housed under controlled humidity and temperature conditions. All the experimental animals were acclimatized for 15 days at 20-26 °C temperature and 30-70 % relative humidity and provided with alternative 12 h light and dark cycle. All standard laboratory requirements

were maintained as per the protocol. Animals were randomized into six groups with three rats in each group. The control group was treated with saline only through intravenous (i.v.) route (tail vein) while the standard group was treated with DXL control at the concentration of 7.5 mg/Kg. The other four groups were treated with respective nanoparticle formulations at the same dose of DXL. Animals were anesthetized and 500 µL of blood was collected in vials containing 3.8 % sodium citrate through retro-orbital plexus at the intervals of 0.5, 1, 2, 4, 8, 12, 24 and 48 h [186]. Then all the samples were centrifuged at 12000 rpm for 10 min. 200 µL of the plasma was separated in vials containing 1 mL of ethyl acetate and vortexed to extract the drug. Then ethyl acetate layers were then separated and kept aside till complete evaporation. 90 µL of mobile phase (acetonitrile, methanol and water in the ratio 45: 45: 10) was mixed with dried ethyl acetate residues and an aliquot of 10 µL was injected into the HPLC column for analysis. A graph of plasma drug concentration against time intervals was plotted.

3.4.8.2. Histopathology study

Wistar rats were used in a histopathology investigation to determine the safety of dual-targeted CS-NPs. Animals were randomly divided into six groups, each with four rats. The i.v. route was used to administered the prepared nanoparticles. The saline control and standard groups were administrated with the saline and DXL (control), respectively. Although, the remaining animal groups (3 to 6) were administrated with DXL-CS-NPs, DXL-CS-F-NPs, DXL-CS-CTXmab-NPs, and DXL-CS-F-CTXmab-NPs at 7.5 mg/kg DXL equivalent dose. The treatment was given three times at a three-day interval, and all the animals were euthanized on the 15th day. The vital organs of all the animals including lungs, liver, kidneys, and heart were taken and stored in the formalin solution (10 % v/v). Afterwards, the specimen was placed in the paraffin box. Using a microtome, specimen

sections were sliced at a thickness of 4 µm. After that, haematoxylin and eosin dyes were used to stain the sections. A light microscope was used to observe the histopathological changes and images were captured [187].

3.4.8.3. Tumour regression and survival analysis

Swiss albino mice weighing 16–20 g were used in the investigation. All the animals were housed in regulated temperature and humidity environments with constant humidity and 12-h light/dark cycle. Randomly, the mice were divided into seven groups (n = 4). Corn-oil was employed as a vehicle to deliver B(a)P orally, and the calculated amount of B(a)P was dissolved using a bath-sonicator. The control group was given an equivalent amount of corn oil for 16 weeks, while the cancer model control group and other groups (3–7) were given B(a)P-corn oil solution at 50 mg/kg. This B(a)P solution was administered twice a week for up to four weeks. After the second week of B(a)P exposure, groups 3 to 7 were given DXL (marketed formulation), DXL-CS-NPs, DXL-CS-F-NPs, DXL-CS-CTXmab-NPs, and DXL-CS-F-CTXmab-NPs through i.v. twice weekly at a dose of 7.5 mg/kg equivalent to DXL control. Afterwards, the animals were sacrificed, and the lungs were collected, preserved in formalin solution (10% v/v), and subjected to histopathological analysis. Haematoxylin dye gives the nuclei a blue colour, while eosin stains the pink colour to the extracellular matrix and cytoplasm. Approximately, 4 µm thick paraffin sections were placed on individual glass slides and stained with hematoxylin and eosin (HE). The bright microscopic images were taken at 10X and the numbers of nuclei were counted in each image by using ImageJ software by separating the blue channels using the "split channels" option. The blue-channel images were then transformed into binary black-and-white images and subsequently processed to estimate the nuclei number. Throughout the study, the health condition of the animals was assessed

every day, and their bodyweights were measured once a week. Kaplan–Meier survival analysis were used to compute the percent survival rate [164,188].

3.5. Results and discussion

3.5.1. Characterization of the CS-F

3.5.1.1 FTIR analysis

The FTIR spectroscopic analysis of folic acid, chitosan, and CS-F was performed (**Figure 3.2)**. The folic acid FTIR spectra demonstrated the stretching frequencies of carbonyl (C=O) and the aromatic C=C group at 1682 cm^{-1} and 1454 cm^{-1} respectively, whereas a characteristic peak of 1-4 disubstituted benzene ring has appeared at 838 cm^{-1}. Moreover, the FTIR spectra of chitosan showed the stretching vibration of the carbonyl group, hydroxyl group (broad peak) and the glycosidic linkage at 1380 cm^{-1}, 3500 cm^{-1} and 1080 cm^{-1} respectively. However, the peaks characteristic of the aromatic C=C group, carbonyl group (C=O) and 1-4 disubstituted benzene ring were devoid in the spectra of CS. Additionally, the spectra of CS-F demonstrated the distinctive peaks of the aromatic C=C, glycosidic bridges (C-O-C bonds) and 1-4 disubstituted benzene ring at 1434 cm^{-1}, 1013 cm^{-1} and 890 cm^{-1} respectively. Since most of the peaks associated with the functional groups of folic acid and CS were found in the FTIR spectra of CS-F with slight changes, the successful conjugation of folic acid to CS can be explained.

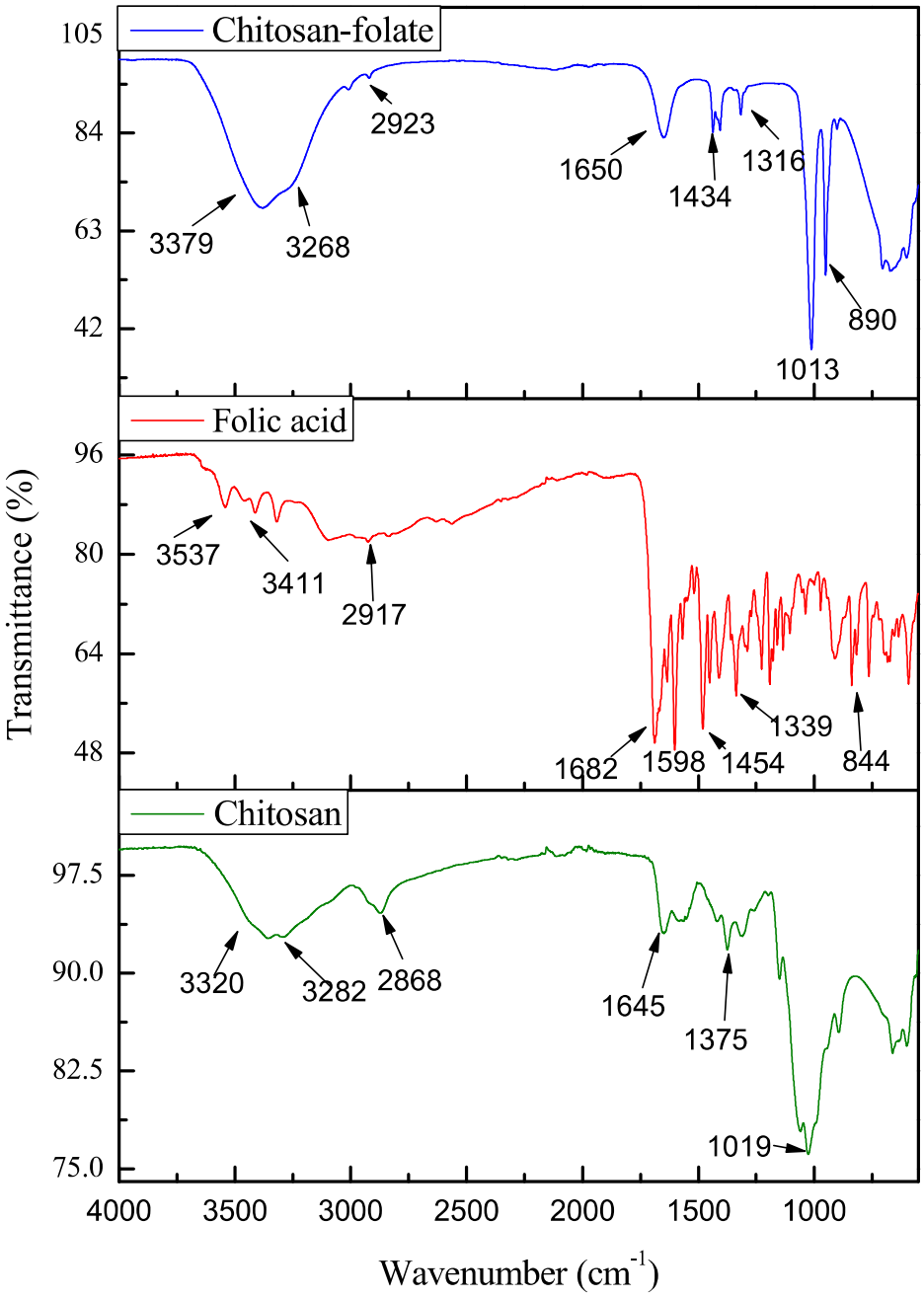

Figure 3.2. FTIR spectra of chitosan, folic acid and chitosan-folate

3.5.1.2. Nuclear magnetic resonance spectroscopy

^{1}H-NMR spectroscopy was used to confirm the synthesis of CS-F conjugate. **Figure 3.3** demonstrated the ^{1}H-NMR spectra of CS and CS-F. However, after the conjugation, the solubility of the CS-F conjugate is reduced in the deuterium oxide, therefore, all the peaks

have not appeared. Although, two distinct peaks of hydrogen proximal to the amide linkage were observed in the spectra of CS-F, indicating the formation of an amide bond. The signal obtained at 2.13 ppm was interpreted for the carbonyl hydrogen next to a carbonyl group (C**H**-CONH), while the peak that appeared at 2.62 ppm can be interpreted as the peak of carbonyl hydrogens connected to nitrogen (R-(CO)-N-C**H**$_2$). Although, the NMR spectra of CS did not show either of these peaks. Likewise, the peaks of the N-**H**$_2$ group of CS appeared between 1.8 and 2.3 ppm, which were missed in the spectra of CS-F, indicating that it was used in the formation of amide bonds.

3.5.1.3. Mass spectroscopy

The synthesized conjugate of the CS-F was analyzed by the TOF mass spectroscopy. (**Figure 3.4**). Since the conjugation process between the amine group of the CS and the carboxylic group of the folic acid resulted in the formation of amide linkages by releasing a molecule of water. The molecular weights of CS and folic acid are 1528 and 441 g/mol, respectively, and therefore the peaks of the CS-F will be higher than the corresponding peaks in the spectra of CS. The molecular ion peak in the spectra of chitosan was appeared at m/z 1528.6, whereas the comparable peak in the spectra of CS-F was observed at m/z 1951.1 which ensure the successful conjugation of the folic acid to the CS.

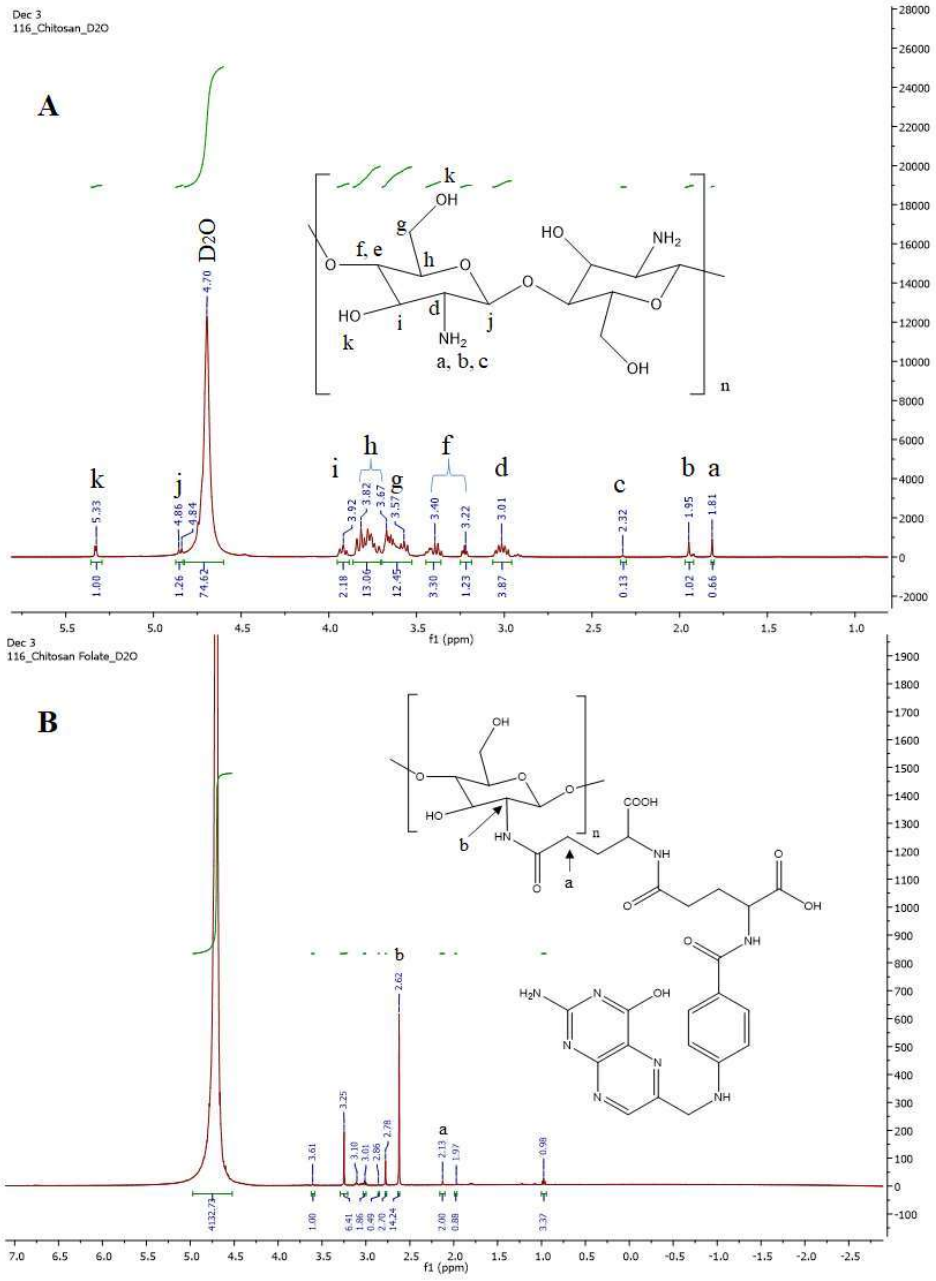

Figure 3.3. ^{1}H-NMR spectrum of A) chitosan and B) chitosan-folate

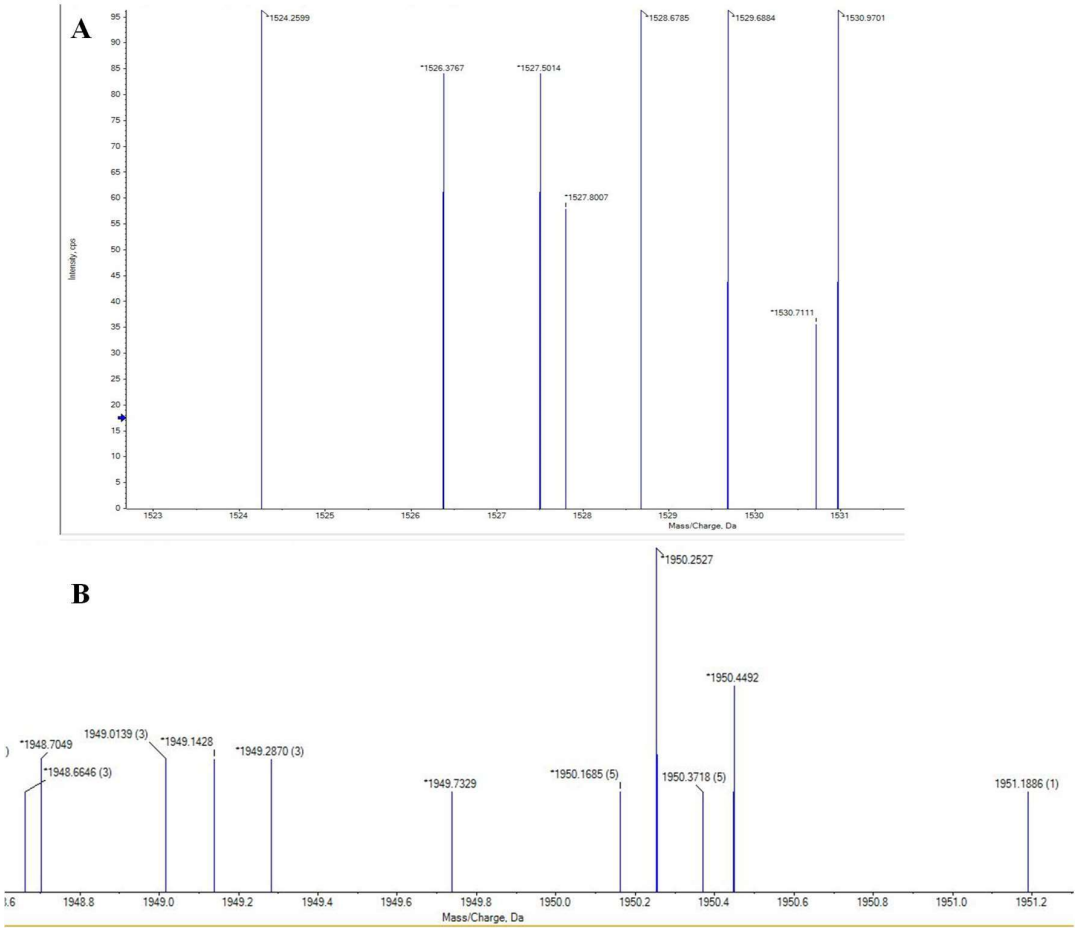

Figure 3.4. Mass spectrum of A) chitosan and B) chitosan-folate

3.5.1.4. Degree of folic acid substitution

The degree of folic acid substitution to the CS was determined by UV spectroscopy, and the results demonstrated that the degree of substitution was 71.3 ± 1.2 %, which is within the acceptable limit.

3.5.2. Characterization of TPGS-COOH

3.5.2.1. FTIR analysis

The synthesized TPGS-COOH was analyzed by the FTIR spectra as shown in **Figure 3.5**. The OH peak of the TPGS-COOH showed a vast characteristic peak, whereas, for TPGS, it is slightly broad. The C=O adsorption band was observed at 1734 cm^{-1} in TPGS spectra whereas it was shifted to 1721 cm^{-1} in TPGS-COOH spectra. However, a typical peak of C-O-C stretching vibrations for the repeating unit of $-OCH_2CH_2$ was identified at 1104 cm^{-1} and 1086 cm^{-1} in the spectra of TPGS and TPGS-COOH, respectively. Furthermore, the aromatic C-C stretching vibration in TPGS spectra was seen at 1413 cm^{-1}, while it was displaced to 1407 cm^{-1} in TPGS-COOH.

3.5.2.2. Nuclear magnetic resonance

The ^{1}H-NMR spectra of TPGS and TPGS-COOH (**Figure 3.6**.) displayed the typical peaks, which implies that the synthesis was successful. All of the peaks were interpreted and assigned to their respective spectrums. The alcoholic proton of TPGS is found at 4.58 ppm, although it is absent from the spectra of TPGS-COOH, indicating that the OH group has been substituted. TPGS-COOH spectra have also revealed the new peaks at 2.37 and 2.98 ppm, identified as the peaks of the methylene group of the conjugated succinic group. However, the peak for the proton of the carboxylic group was not observed; therefore, the presence of the carboxylic group was again confirmed by the ^{13}C-NMR analysis (**Figure 3.7**). The ^{13}C spectra of the TPGS showed two characteristic peaks of the carbonyl carbons (C=O) at 171.1 ppm and 172.43 ppm. Whereas the spectra of TPGS-COOH showed four distinct peaks of the carbonyl carbons (two additional carbonyl carbons of the conjugated succinic group) observed at 171.1 ppm, 172.4 ppm, 173.8 ppm and 174.6 ppm, which ensure the synthesis of the TPGS-COOH.

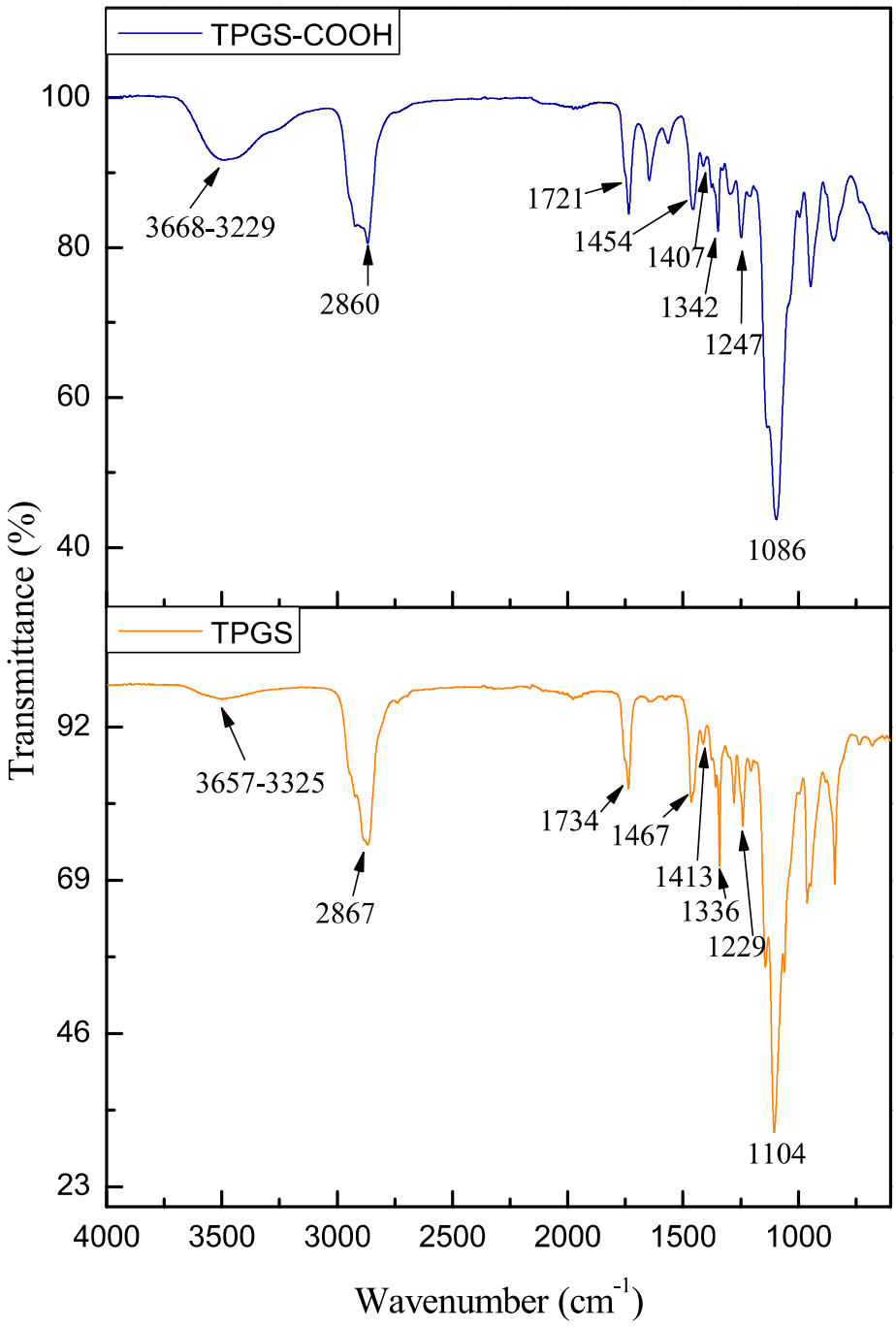

Figure 3.5. FTIR spectra of TPGS and TPGS-COOH

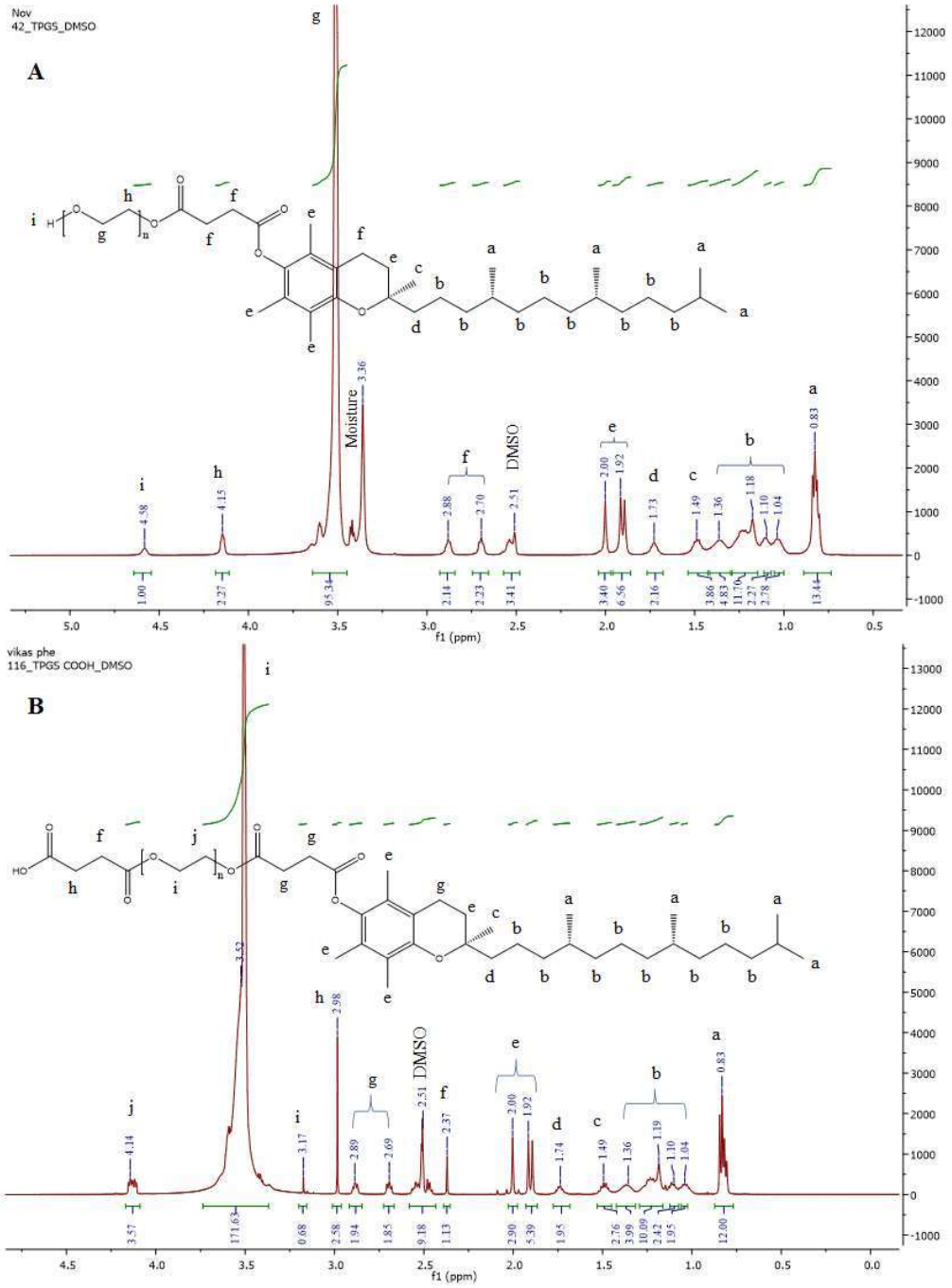

Figure 3.6. [1]H-NMR spectrum of A) TPGS and B) TPGS-COOH

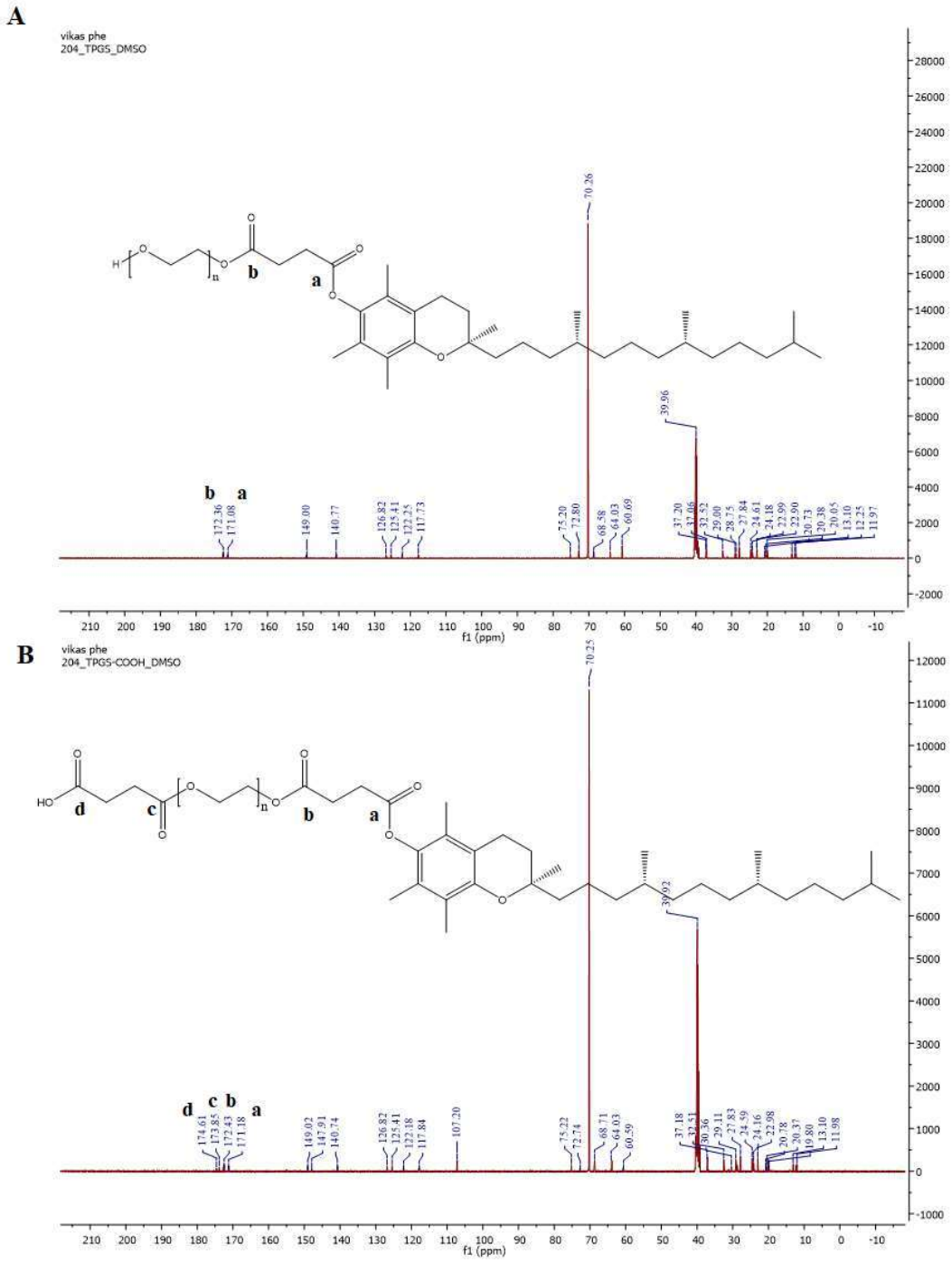

Figure 3.7. ^{13}C-NMR spectra of the A) TPGS and B) TPGS-COOH showing the peaks of the carbonyl carbons

3.5.2.3. Mass spectroscopy

TOF mass spectrometry was used to ensure the synthesis of TPGS-COOH **(Figure 3.8).** Since the structure of TPGS and TPGS-COOH contains a considerable number of oligomers (-OCH_2CH_2-, m/z = 44), their spectra predominantly displayed the peaks of doble charged species at half of their original molecular mass (m/z 44/2= 22). Furthermore, peaks for singly charged species also appeared, supporting the successful modification of the TPGS. Since succinic anhydride was utilized as the key reactant for the carboxylation of the TPGS, the mass spectra of TPGS-COOH showed comparable peaks higher than 101 units than the mass spectra of TPGS. The mass spectra of TPGS-COOH showed a base peak at m/z 551, and the TPGS mass spectra also showed a definite fragmentation peak at m/z 450, (peak difference of 101 units), indicating that the TPGS was successfully modified. Furthermore, multiple peaks appeared in the mass spectrum of the TPGS at m/z 532, 760, and 1455 and their comparable peaks (plus 101 units) have appeared in the mass spectrum of the TPGS-COOH at m/z 633, 861, and 1557 respectively. Although, for the doubly charged ion species, the peak difference in the mass spectra of TPGS-COOH should be approximately 50.5 units greater than the respective peaks in the mass spectrum of the TPGS. However, the multiple peaks for doubly charged ion species were identified in the mass spectrum of the TPGS at m/z 560.3, 684.9, 706.4, 728.4, 750.5, 794.5, 816.3, 817.0, 835.5, 882.5 and 1027, whereas their corresponding peaks were identified in the mass spectrum of the TPGS-COOH at m/z 611.3, 734.9, 756.9, 778.9, 800.4, 844.5, 866.5, 867.0, 888.5, 933.4, 1557.9 respectively. All of these findings demonstrated that the TPGS-COOH was successfully synthesized.

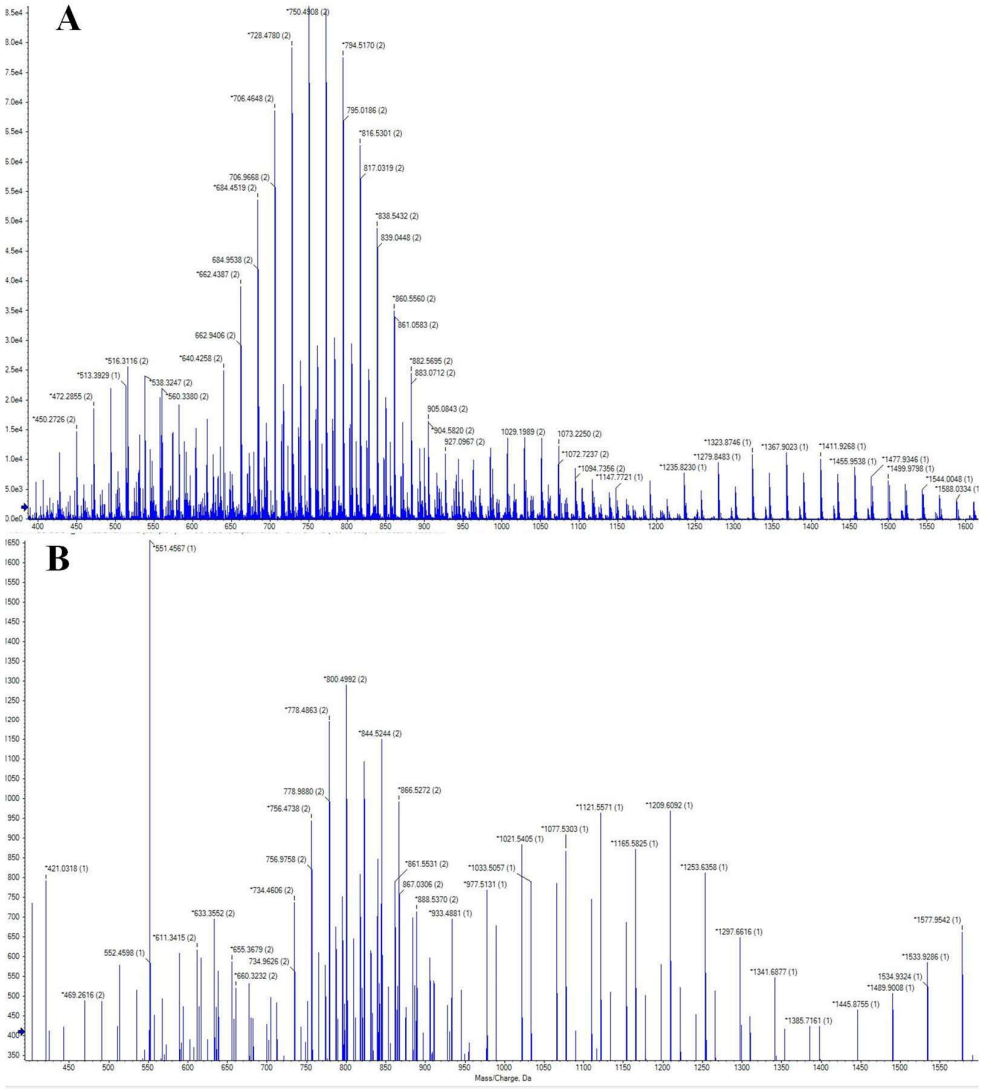

Figure 3.8. Mass spectrum of A) TPGS and B) TPGS-COOH.

3.5.3. Particle size distribution and surface charge

Table 3.2. shows the physicochemical evaluation parameters of CS-NPs. The hydrodynamic diameter values of prepared formulations were in the range of 119.0 ± 7.18 nm to 156.0 ± 4.47 nm. The particle size analysis suggested that all the nanoparticle formulations were in the size range of 120 to 200 nm. The ligand conjugation onto the surface of nanoparticles resulted in a significant increase in particle size ($p<0.05$). The

surface charge of non-targeted CS-NPs (DXL-CS-NPs) was observed to be 16.40 ± 2.56 mV, which was reduced after the conjugation with folic acid (DXL-CS-F-NPs) up to -2.0 ± 3.65 mV whereas in the case of DXL-CS-CTXmab-NPs and DXL-CS-F-CTXmab-NPs, it was further reduced up to 3.89 ± 1.36 mV, and -0.80 ± 0.99 respectively. The reason may be due to the negative surface charge associated with cetuximab which made the surface of targeted NPs less positive.

3.5.4. TEM analysis

The shape, constitutive structure and morphology of the nanoformulations were analyzed by transmission electron microscopy. **Figure 3.9.A.** depicts the TEM images of nanoparticles with 100 nm and 200 nm scale. In the images with 100 nm scale, the individual particles can be interpreted to be spherical without any major surface defects such as pits and crevices. However, the image with a 200 nm scale showed the monodispersed spherical particles.

3.5.5. SEM analysis

The shape and size of the non-targeted, single ligand as well as dual ligand decorated nanoparticles were characterized by scanning electron microscopy (Fei Company of USA (S E a) Pte Ltd.). From the **Figure 3.9.B**, the images illustrated that the sizes of all prepared nanoparticles were in the range of 200 nm, spherical in shape, monodispersed and smooth surface with no noticeable pinholes/cracks. Moreover, the particle size data from DLS studies was in absolute agreement with that of observed from SEM and TEM data.

Table 3.2. Physicochemical parameters and IC_{50} values of DXL- CS-NPs, DXL-CS-F-NPs, DXL-CS-CTXmab-NPs and DXL-CS- F-CTXmab-NPs

Batches	Particle Size (mean ± SD*)	Polydispersity index (mean ± SD*)	Zeta potential (mean ± SD*)	Entrapment efficiency (%) (mean ± SD*)	IC_{50}Value (mean ± SD*)
DXL(Control)	-	-	-	-	27.45 ± 0.88
DXL- CS-NPs	119.0 ± 7.18	0.217 ± 0.08	16.40 ± 2.56	75.0 ± 1.63	18.70 ± 1.62
DXL-CS-F-NPs	122.9 ± 5.28	0.242 ± 0.04	-2.0 ± 3.65	70.83 ± 0.98	15.48 ± 2.69
DXL-CS-CTXmab-NPs	126.4 ± 8.12	0.294 ± 0.06	3.89 ± 1.36	62.5 ± 2.81	7.36 ± 2.03
DXL-CS-CTXmab-F-NPs	156.0 ± 4.47	0.241 ± 0.07	-0.80 ± 0.99	61.33 ± 1.92	0.81 ± 1.45
C6- CS-NPs	120.4 ± 3.21	0.254 ± 0.09	13.80 ± 2.58	73.9 ± 3.17	-
C6- CS-F-NPs	125.0 ± 2.33	0.300 ± 0.03	-2.21 ± 4.01	72.5 ± 1.24	-
C6- CS-CTXmab-NPs	132.1 ± 3.42	0.281 ± 0.09	7.63 ± 1.65	69.82 ± 0.96	-
C6- CS-CTXmab-F-NPs	141.0 ± 5.23	0.312 ± 0.05	-1.78 ± 3.85	65.45 ± 2.96	-

values of nanoparticles (NPs)
*n = 3
S.D: Standard deviation
DXL-CS-NPs: DXL loaded CS-NPs
DXL-CS-F-NPs: DXL loaded folate-receptor targeted CS-NPs
DXL-CS-CTXmab-NPs: DXL loaded EGFR targeted CS-NPs
DXL-CS-CTXmab-F-NPs: DXL loaded dual-receptor targeted CS-NPs
C6- CS-NPs: C6 entrapped chitosan NPs
C6- CS-F-NPs: C6 entrapped folate-receptor targeted CS-NPs
C6- CS-CTXmab-NPs: C6 entrapped EGFR targeted CS-NPs
C6- CS-CTXmab-F-NPs: C6 loaded dual-receptor targeted CS-NPs

3.5.6. AFM analysis

The surface topology and size of nanoparticle formulations were characterized by atomic force microscopy. 2-D and 3-D AFM images from **Figure 3.9.C and D** are revealing the fact that particles are spherical in shape and smooth surfaced without any obvious pinholes and cracks. All the formulations were seem to have the particle sizes below 200 nm which are also quite comparable to the values obtained from particle size analysis.

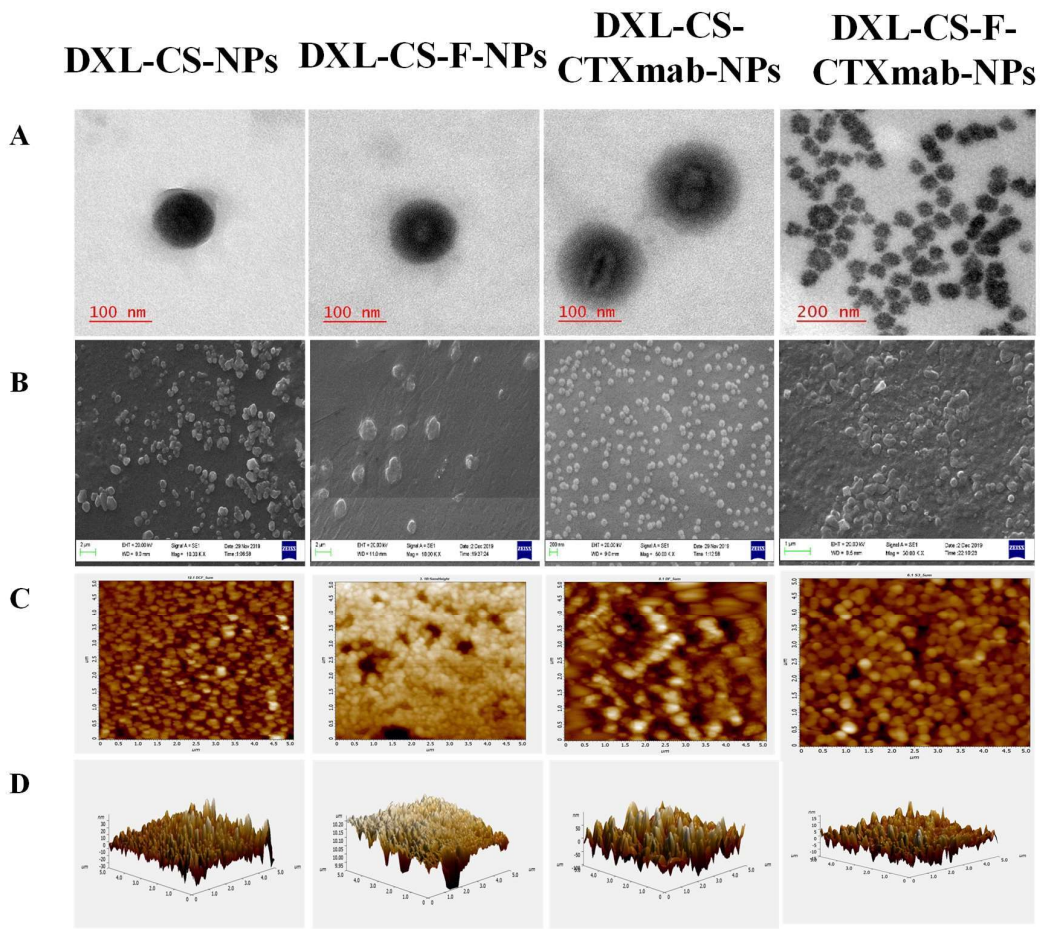

Figure 3.9. A) Transmission electron microscopic images, B) scanning electron microscopic images and, C) 2-D and D) 3-D atomic force microscopic images of non-targeted, folate-receptor, EGFR and dual-receptor targeted CS-NPs

3.5.7. Drug entrapment efficiency of nanoparticles

The % DXL entrapment of the non-targeted, folate-receptor, EGFR and, dual-receptor targeted CS-NPs was found to be 75.0 ± 1.63 %, 70.83 ± 0.98 %, 62.5 ± 2.81 % and 61.33 ± 1.92 % respectively (table 2). The extent of conjugation (single or dual ligand decorated) to the nanoparticle formulation interferes in the drug entrapment. The entrapment efficiency of dual-ligand targeted nanoparticles was slightly lesser than single-ligand targeted and non-targeted nanoparticles [162]. The C6 entrapment efficiency of the non-targeted, folate targeted, EGFR targeted and dual receptor targeted

NPs was found to be 73.9 ± 3.17%, 72.5 ± 1.24 and 69.82 ± 0.96%, and 65.45 ± 2.96 % (**Table 3.2**) respectively.

3.5.8. X-ray diffraction (XRD) analysis

The physical state of the nanoparticle was evaluated by XRD analysis (**Figure 3.10**). The XRD spectra of the DXL showed sharp peaks which revealed its crystalline nature. The peaks observed in the XRD spectra DXL-CS-NPs, DXL-CS-FNPs, DXL-CS-CTXmab-NPs, DXL-CS-F-CTXmab-NP did not match with the XRD peaks of DXL, indicating that the drug is successfully loaded in the formulations. Whereas, the XRD spectra of DXL-CS-NPs showed broad peaks and numerous well-defined sharp peaks. However, similar sharp peaks have also appeared in the XRD spectra of CZT-CSA-F-NPs with a lesser intensity which revealed their semi-crystalline characteristics. Since the distribution of chitosan, alginate, and Na-TPP in the polyelectrolyte complex is consistent throughout the nanoparticles, and some Na-TPP content may be retained on the surface of nanoparticles. Therefore, the Na-TPP may be responsible for the sharp crystalline peaks observed in the XRD spectra of the DXL-CS-NPs and DXL-CS-F-NPs. Contrastingly, the XRD spectra of DXL-CS-CTXmab-NPs and DXL-CS-F-CTXmab-NPs displayed no sharp peaks, which can be correlated with the presence of the targeting ligands, i.e., folate and CTXmab. Hence, the XRD analysis revealed the physical state of the CSA-NPs with the evidence of the coating with the targeting ligands.

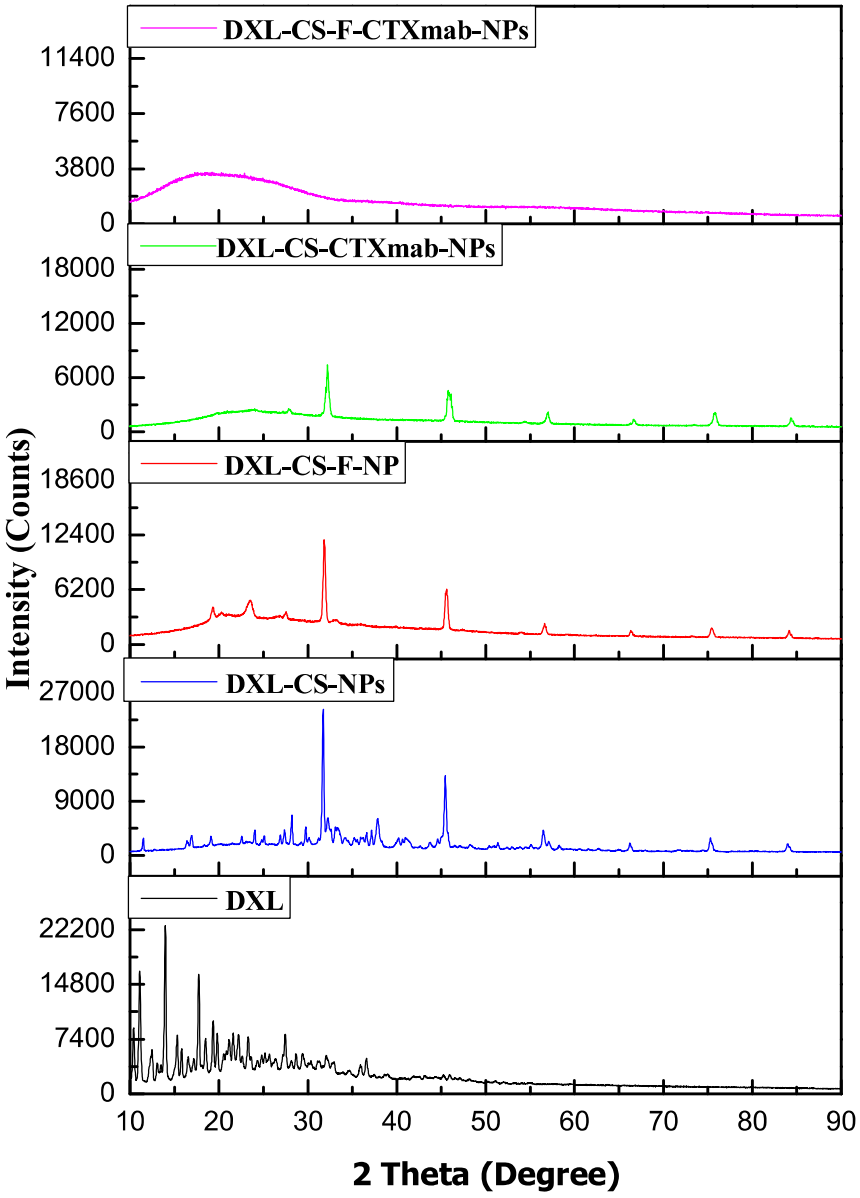

Figure 3.10. XRD spectra of DXL, non-targeted, folate-receptor, EGFR and dual-receptor targeted CS-NPs

3.5.9. XPS analysis

The surface chemistry of DXL-CS-NPs, DXL-CS-F-NPs, DXL-CS-CTXmab-NPs, DXL-CS-F-CTXmab-NPs was studied by X-ray photoelectron spectroscopy (XPS). The XPS spectra showed the characteristic peaks for elements C, O and N and are depicted in **Figure 3.11**. The percentage of N 1s, O 1s and C 1s in DXL-CS-NPs was 1.04 ± 0.23 %,

15.19 ± 1.24 % and 83.77 ± 3.21 % respectively, whereas for DXL-CS-F-NPs, these were 5.8 ± 0.89 %, 27.76 ± 3.24 % and 66.44 ± 1.24 %. This significant increase in the percentage of N 1s and O 1s in DXL-CS-F-NPs indicated the presence of folic acid on the surface of nanoparticles since the percentage of respective elements was very less in DXL-CS-NPs, which only implied the coating of TPGS. The successful post conjugation of cetuximab was also confirmed by the XPS study. The percentage of N 1s, O 1s and C 1s in DXL-CS-CTXmab-NPs were 9.74 ± 0.89 %, 22.54 ± 2.32 % and 67.74 ± 3.65 % respectively, while for DXL-CS-F-CTXmab-NPs, the percentages were 11.53 ± 0.22 %, 24.01 ± 2.37 % and 64.46 ± 4.32 % respectively. **Figure 3.11.B.** demonstrated that, the percentage of nitrogen in DXL-CS-F-CTXmab-NPs was significantly higher than non-targeted and folate receptor targeted NPs, which can be attributed to the presence of the large number of nitrogen atoms, (N = 1732) in cetuximab whereas it is slightly higher than DXL-CS-CTXmab-NPs, due to the presence of folic acid (N = 7). Therefore, the distinguishable intensities of nitrogen, oxygen and carbon in the XPS survey indeed confirmed the presence of cetuximab and folic acid on the surface of DXL-CS-F-CTXmab-NPs. An additional peak observed at 500 eV is the characteristic for the Na KLL or Na 2s, which may be due to the Na-TPP, a crosslinker used in the preparation of CS-NPs. Na KLL auger peak was observed in the XPS survey of the non-targeted (DXL-CS-NPs) nanoparticles. But it was very less or absent in the other single targeted and dual-targeted CS-NPs. It is vanished in the targeted nanoparticles, because of the possible covering by the targeting ligands.

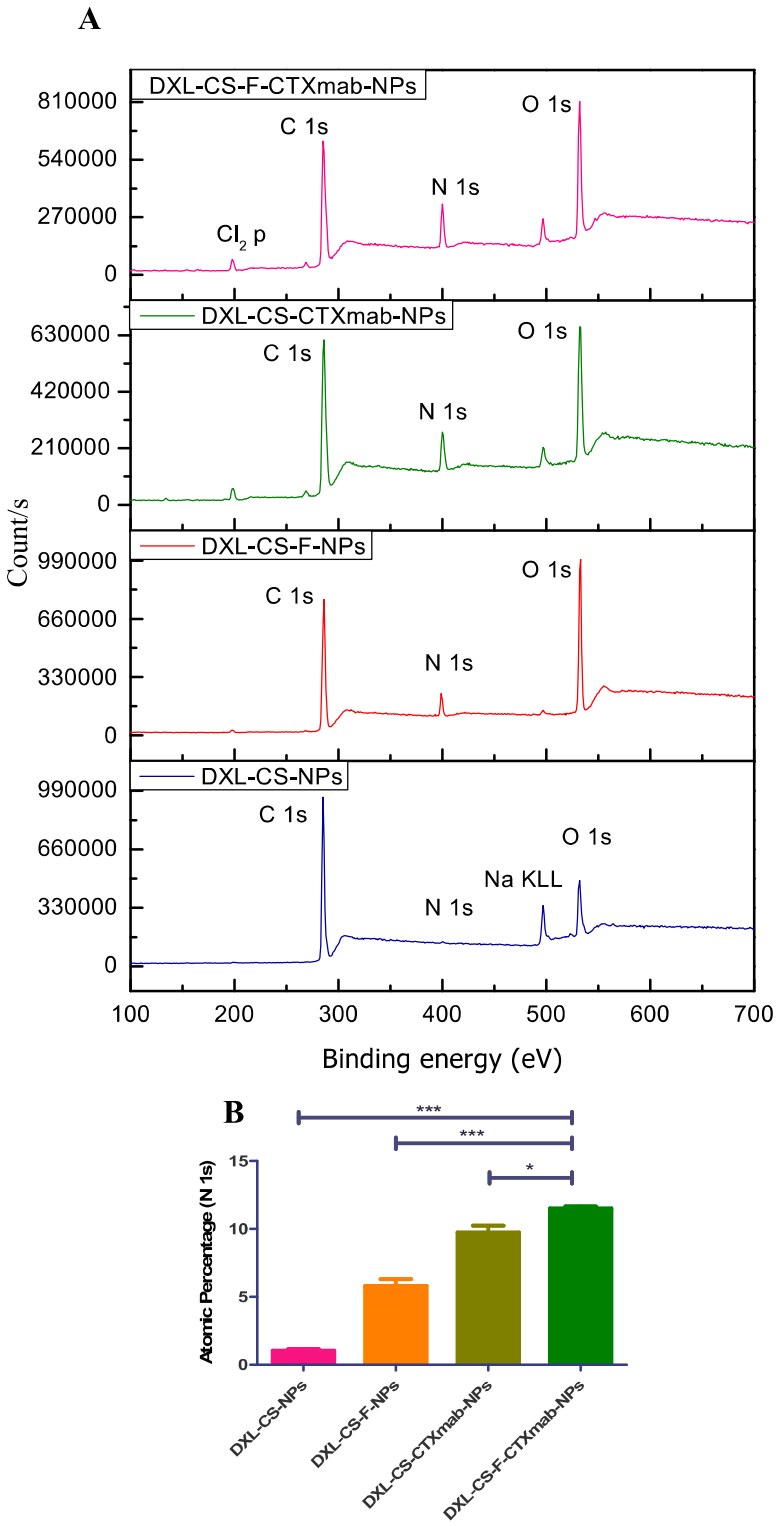

Figure 3.11. A) XPS spectra of non-targeted, folate-receptor, EGFR and dual-receptor targeted CS-NPs, B) atomic percentafe of nitrogen atoms (N 1s)

3.5.10. Degree of conjugation

3.5.10.1. Folic acid

The folic acid content in DXL-CS-F-NPs and DXL-CS-F-CTXmab-NPs was 68.3 ± 3.0 % and 66.6 ± 2.3 %, respectively. The presence of CTXmab on the surface of DXL-CS-F-CTXmab-NPs can justify the reduction of the folic acid content.

3.5.10.2. CTXmab

The extent of conjugation of cetuximab on the surface of single EGFR targeted and dual-receptor targeted CS-NPs was determined by Bradford assay and the results revealed that approximately 71.53 ± 5.81 % of cetuximab surface conjugation was achieved in EGFR targeted CS-NPs. In dual targeted NPs, it was 67.32±4.03 %. The reason for this slight decrease in case of dual targeted CS-NPs may be the reduction of the available surface area due to the presence of folate residues.

3.5.11. In-vitro evaluation

3.5.11.1 In-vitro release study

The release profiles of DXL from non-targeted, folate-receptor, EGFR and, dual-receptor targeted CS-NPs were studied in PBS pH 5.5 and pH 7.4 and the results are illustrated in **Figure 3.12**. The release of DXL from formulations followed the biphasic release pattern (burst release followed by sustained release); almost in all the formulations, 50 % of drug was released within 8 to 12 h with different rates (which may act as loading dose), followed by sustained release up to 72 h (that maintained the desired levels). The extent of drug release in PBS pH 5.5 was higher than that of in pH 7.4 **(Figure 3.12. B and C)**. Higher drug release from all nanoparticle formulations in acidic media can be attributed to its isoelectric point (CS, 6.3); at pH below its isoelectric point, the amino group of the chitosan gets protonated and swollen, consequently facilitating faster dissolution of CS.

As tumor usually possesses acidic microenvironment, CS-NPs would be expected to release the drug exclusively in the cancer cells. The percentage of DXL released from non-targeted, folate targeted, EGFR targeted and dual receptor targeted NPs in PBS (pH 5.5) after 72 h, was 99.06 ± 0.46 %, 98.13 ± 0.56 %, 95.49 ± 0.77 %, and 95.12 ± 0.71 % respectively.

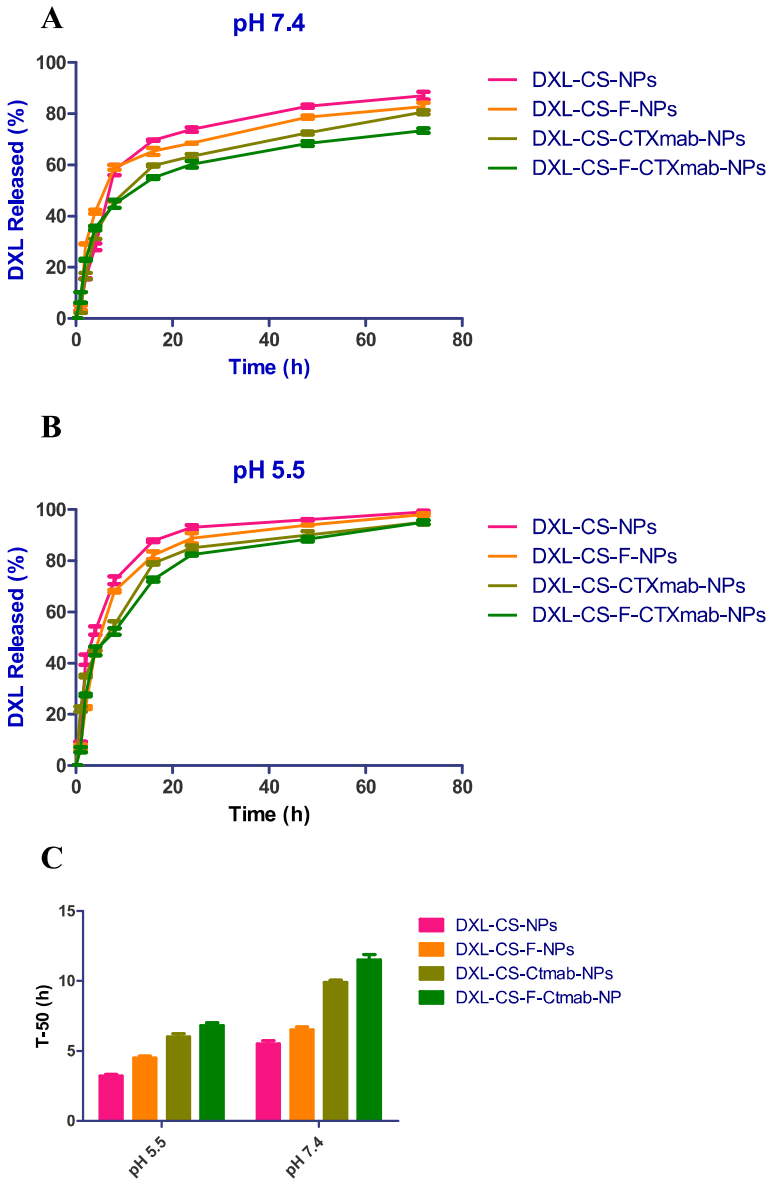

Figure 3.12. Drug release profile of DXL in CS-NPs in A) PBS pH 7.4, B) PBS pH 5.5, and C) histogram showing T_{50} (h) values

3.5.11.2. In-vitro cellular uptake study

To compare the synergistic effect of folate and cetuximab dual ligand surface conjugation on the extent of cellular uptake in comparison to non-targeted and single ligand decorated formulations, cellular uptake study of C6 loaded nanoparticles was carried out on A-549 cells, and the respective images were captured with a fluorescence microscope. To get the commensurate and accurate results based on the intensity of fluorescence, images of the treated cells were taken with similar parameters such as offset, gain, sensitivity and laser power constant throughout the imaging process. The confocal fluorescent images of nanoparticles were obtained with the differentiable green channel (C6), blue channel (DAPI) and merge of both channels (**Figure 3.13**). The green channel represents the internalization of C6 loaded nanoparticles, and the fluorescence intensity was quantified using image-J software by detecting the percentage area of the green channels **(Figure. 3.14. C).** The percentage area of green channels of confocal images of pure C6, C6 loaded non-targeted, folate targeted, EGFR targeted and dual receptor targeted NPs was 3.88 ± 0.51, 5.63 ± 0.45, 6.05 ± 0.28, 6.7 ± 0.3 and 10.2 ± 0.6 respectively. C6-CS-CTXmab-F-NPs showed the highest percent area of green channels which was almost 2.6, 1.8, 1.6, 1.5 times higher than pure C6, C6-CS-NPs, C6-CS-F-NPs and C6-CS-CTXmab-NPs respectively. These results demonstrated the substantial increment in the cellular uptake of the dual-targeted nanoparticles in A-549 cell lines. Enhanced cellular uptake can also be correlated with the common endocytic pathway (via-caveolae) through folate and EGFR [189].

3.5.11.3. Cytotoxicity studies

Here, A-549 (human adenocarcinoma) and SIRC (control) cells were used to evaluate the cytotoxicity of folate and cetuximab dual -ligand decorated CS-NPs. It was well reported

in previous studies that folate receptor-1 and EGF receptors are overexpressed in A-549 cells [190]. **Figure 3.14. A** shows the percent cell viability after treatment with DXL loaded non-targeted, folate targeted, EGFR targeted and dual receptor targeted NPs in contrast to DXL control at comparable DXL concentrations. The % cell viability was lower with DXL-CS-NPs in comparison to DXL control which can be correlated to enhanced cellular uptake and bio adhesion property of CS-NPs. Again, a further remarkable decrease in the cell viability was observed with DXL-CS-F-NPs, DXL-CS-CTXmab-NPs, and DXL-CS-F-CTXmab-NPs with respect to to DXL-CS-NPs. The enhanced cytotoxicity of DXL-CS-CTXmab-NPs and DXL-CS-F-NPs may be due to the targeted active delivery of DXL loaded nanoparticles in addition to EGFR as well as folate mediated endocytosis. The molecular mechanism of endocytosis for both of these targeting agents is the caveolar based endocytosis which involves the bulb-shaped, plasma membrane invaginations called caveolae.

In the nanoparticles formed by the folate cross-linked chitosan, folate is usually distributed on their surface as well as in the inner part of the nanoparticles, since the CS-NPs are characterized by the cross-linked network in the polymer backbone. The formulation having both, folate and cetuximab surface decoration showed the highest cytotoxicity and lowest IC_{50} values among all the formulations. These results supported the hypothesis of synergistic uptake of the nanoparticles by folate as well as EGFR mediated endocytosis. An increase in drug concentration from 0.025 µg/mL to 25 µg/mL also increased the cytotoxicity of DXL-CS-F-CTXmab-NPs by virtue of the dual-receptor targeted mechanism. IC_{50} values for non-targeted, folate targeted, EGFR targeted and dual receptor targeted NPs vs DXL control are 18.70 ± 1.62, 15.48 ± 2.69, 7.36 ± 2.03 and 0.81 ± 1.45 vs 27.45 ± 0.88 µg/mL of DXL control. These results suggest that dual ligand

targeted CS-NPs have significantly enhanced the cytotoxicity of A-549 cells. Since, SIRC cells are not malignant, folate and EGF receptors are less expressed. Therefore, the CS-NPs, exhibited reduced cytotoxicity against SIRC cells. Hence, the findings suggested that, the dual-targeted CS-NPs may useful for effective treatment of lung cancer.

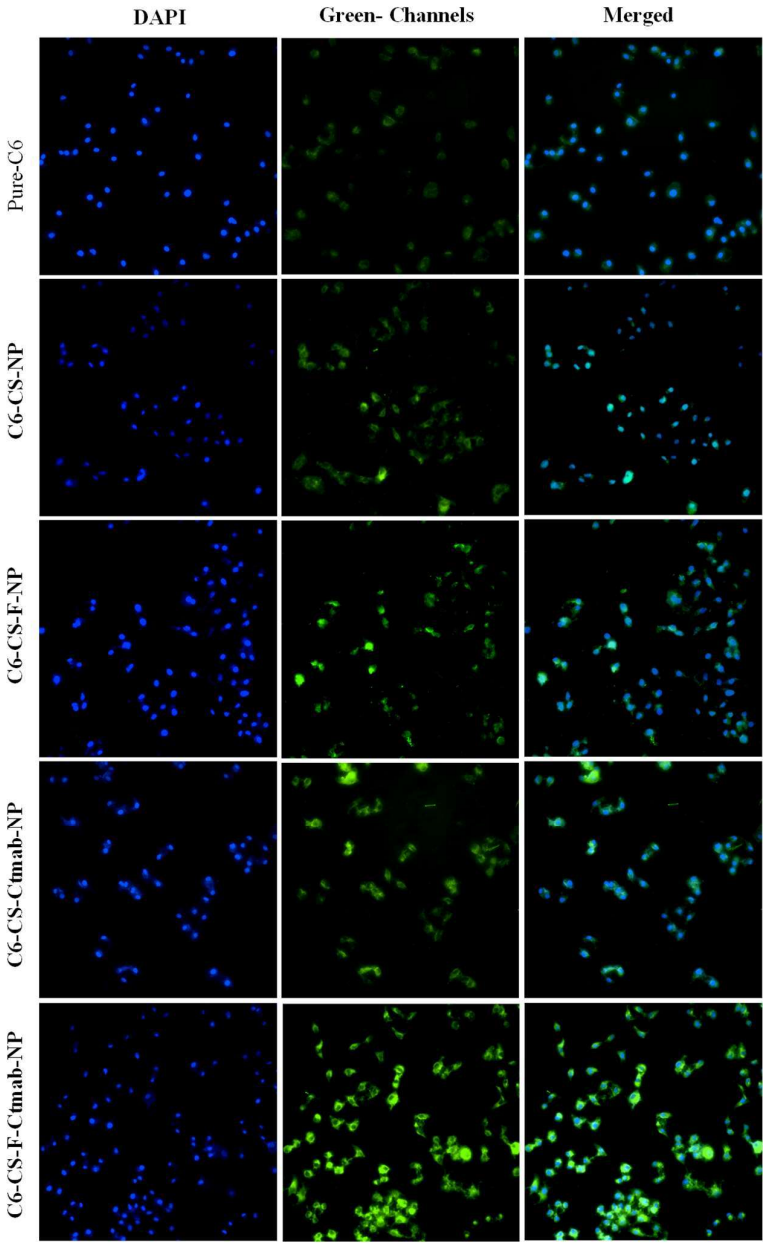

Figure 3.13. *In-vitro* cellular uptake study of C6 loaded non-targeted, folate-receptor, EGFR and, dual-receptor targeted CS-NPs against A-549 cells

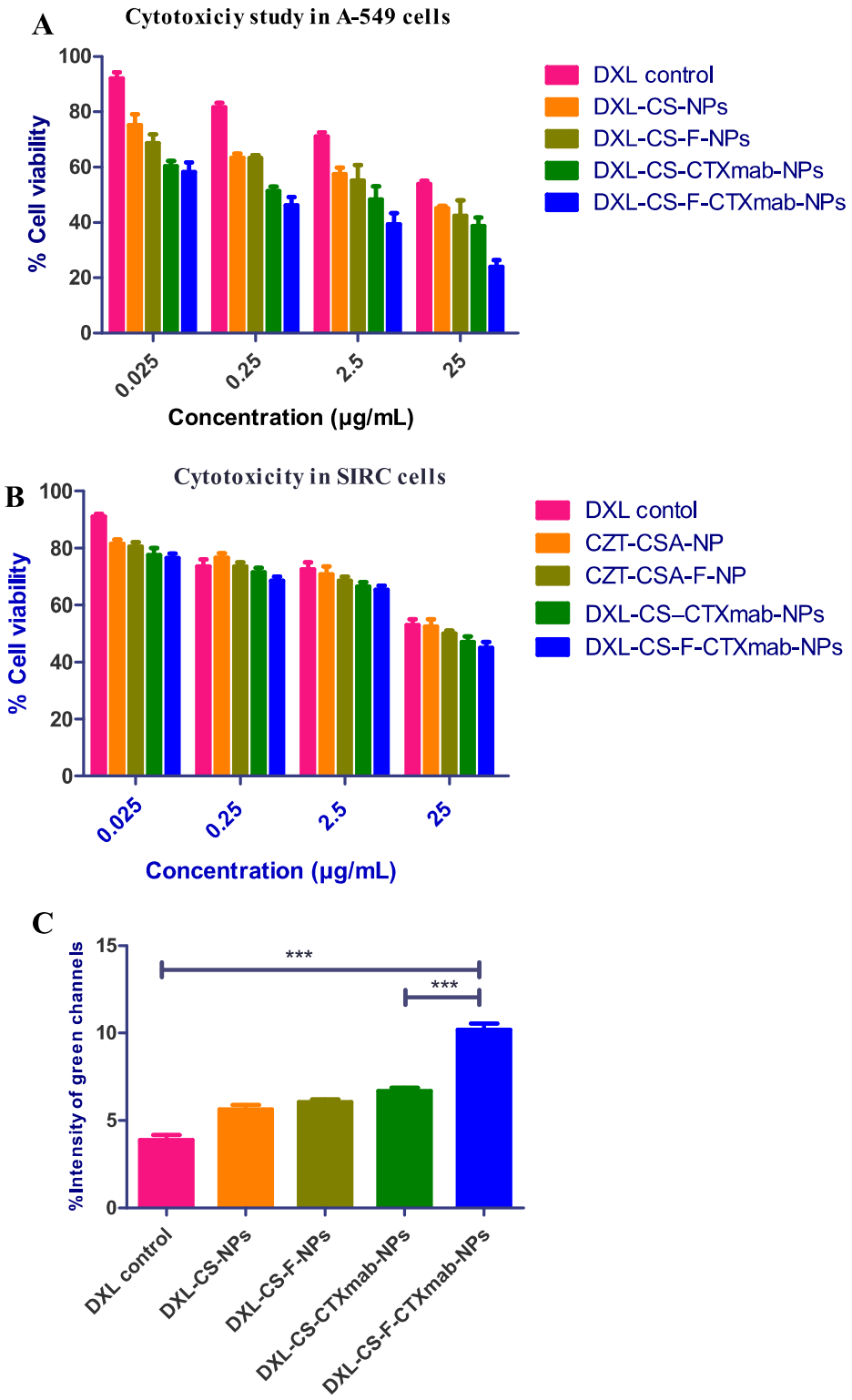

Figure 3.14. Graph showing the percent cell viability after 24 h incubation with A) A-549 cells B) SIRC cells. C) histogram showing the percent intensity of the green channels in cellular-uptake images in A-549 cells

3.5.12. In-vivo characterization

3.5.12.1. Pharmacokinetic study

In-vivo pharmacokinetic study of DXL control, non-targeted, folate targeted, EGFR targeted and dual receptor targeted NPs was performed on Wistar rats. The plasma DXL concentration versus time plot was obtained (**Figure 3.15**) after i.v. administration of formulations at 7.5 mg/kg equivalent concentrations of DXL. The results demonstrated approx. three times higher relative bioavailability of non-targeted, folate targeted, EGFR targeted and dual receptor targeted NPs in comparison with DXL control. The pharmacokinetic profile of DXL-CS-F-CTXmab-NPs also showed increased half-life and mean residence time as compare to DXL control ($p<0.05$). Nanoparticle formulations other than DXL control showed a significant lower clearance rate (**Table 3.3**). The improved DXL residence time and half-life in the body may be due to the stealth effect conferred by surface modification with PEG containing TPGS which prevents opsonization and thus accomplishing its role as a long circulatory formulation in addition to inhibition of multi-drug resistant P-gp efflux pump.

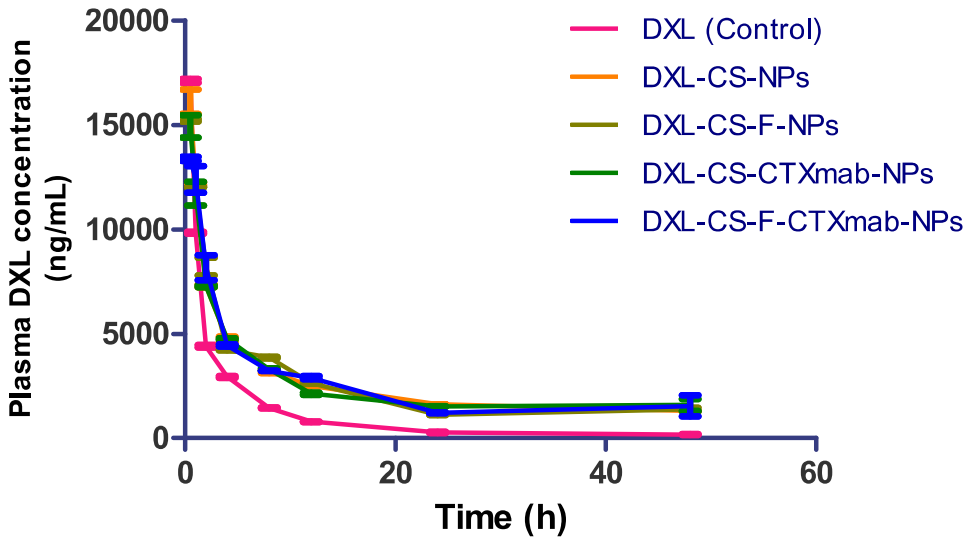

Figure 3.15. Pharmacokinetic analysis of DXL control, non-targeted, folate targeted, EGFR targeted and dual receptor targeted NPs after i.v. administration (7.5 mg/kg, n = 3) in Wistar rats

Table 3.3. Pharmacokinetic parameters of DXL control, non-targeted, folate targeted, EGFR targeted and dual receptor targeted NPs after i.v. administration at 7.5 mg/kg equivalent concentration of DXL

Pharmacokinetic parameters	DXL control (mean ± SD*)	DXL-CS-NPs (mean ± SD*)	DXL-CS-F-NPs (mean ± SD*)	DXL-CS-CTXmab-NPs (mean ± SD*)	DXL-CS-F-CTXmab-NPs (mean ± SD*)
AUC_{total} (ng.h/ml)	33675 ± 3061	67283 ± 2748	61294 ± 2947	58078 ± 3527	58801 ± 2224
C_{max} (ng/ml)	17005 ± 251	15878 ± 585	15175 ± 369	14750 ± 591	14830 ± 385
T_{max} (h)	0.5	0.5	0.5	0.5	0.5
$T_{1/2}$(h)	15.4 ± 2.01	41.01 ± 10.58	48.05 ± 3.65	50.76 ± 3.30	53.74 ± 5.80
MRT(h)	10.31 ± 1.61	49.77 ± 3.21	57.43± 3.22	64.09 ± 4.36	68.81 ± 4.32
V_d (l/kg)	0.44 ± 0.06	0.47 ± 0.09	0.49 ± 0.07	0.50 ± 0.10	0.50 ± 0.12
CL_T (ml/kg.h)	19.8 ± 2.3	7.94 ± 3.2	7.06 ± 2.7	6.82 ± 2.6	6.44 ± 1.3
F_R	-	3.28 ± 0.8	3.26 ± 1.2	3.32 ± 0.9	3.26 ± 1.4f

*n = 3
DXL-CS-NPs: DXL loaded CS-NPs
DXL-CS-F-NPs: DXL loaded folate-receptor targeted CS-NPs
DXL-CS-CTXmab-NPs: DXL loaded EGFR targeted CS-NPs
DXL-CS-CTXmab-F-NPs: DXL loaded dual-receptor targeted CS-NPs
MRT: Mean residence time
V_d: Volume of distribution
CL_T: Total body clearance
F_R: Relative bioavailability

3.5.12.2. Histopathological analysis

After multiple administrations, the heart, lung, liver, and kidney of Wistar rats treated with the saline control showed no pathological abnormalities (**Figure 3.16**). DXL control animals had loosely arranged cardiac fibres and widespread hepatocyte necrosis regions. The inclusion of tween-80 and ethanol in the marketed formulation of DXL, resulted in significant lesions, indicating toxicity. Despite, the animals treated with DXL-CS-NPs, DXL-CS-F-NPs, DXL-CS-CTXmab-NPs, and DXL-CS-F-CTXmab-NPs only exhibited partial lesions on histological examination. Consequently, the biosafety of CS-NPs was proven adequate compared to a commercially available DXL formulation.

3.5.12.3. Tumour regression and survival analysis

Since tumour tissues have a higher cell count than normal cells, which is a distinguishable trait, as a result, assessing the cell number can reveal the extent of malignancy. Therefore, in this work, by determining the number of nuclei, the anticancer efficacy of all nanoparticle samples in contrast to the control group was analyzed **(Figure 3.17. A and 3.17. B)**. The number of nuclei in the microscopic images of the B(a)P treated group (cancer model control) was 10,338 ± 589, which was significantly higher ($p < 0.001$) than the control group **(Figure 3.17. C)**. However, the number of nuclei in the treatment groups of DXL-CS-NPs, DXL-CS-F-NPs, DXL-CS-CTXmab-NPs, and DXL-CS-F-CTXmab-NPs was 7,867 ± 208, 6650 ± 346, 6067 ± 321, 5733 ± 568, and 4300 ± 300, respectively. The number of nuclei in the microscopic images of the dual-receptor targeted nanoparticles treated group was significantly lower ($p < 0.001$). The dual receptor-targeted CS-NPs treatment group showed a substantially lower nucleus number than the folate and cetuximab targeted formulations, indicating its synergic effect due to enhanced internalization in cancer cells. The Kaplan-Meier survival analysis **(Figure 3.17. D)** revealed the per cent survival of lung cancer induced mice treated with DXL-CS-NPs, DXL-CS-F-NPs, DXL-CS-CTXmab-NPs, and DXL-CS-F-CTXmab-NPs is significantly prolonged as compared with cancer model control. The dual-receptor targeted nanoparticles treated group had the best survival rate compared to the other treatment groups. As a result, when compared to other formulations, the dual-targeted chitosan nanomedicine showed the highest anticancer activity and prolonged survival rate.

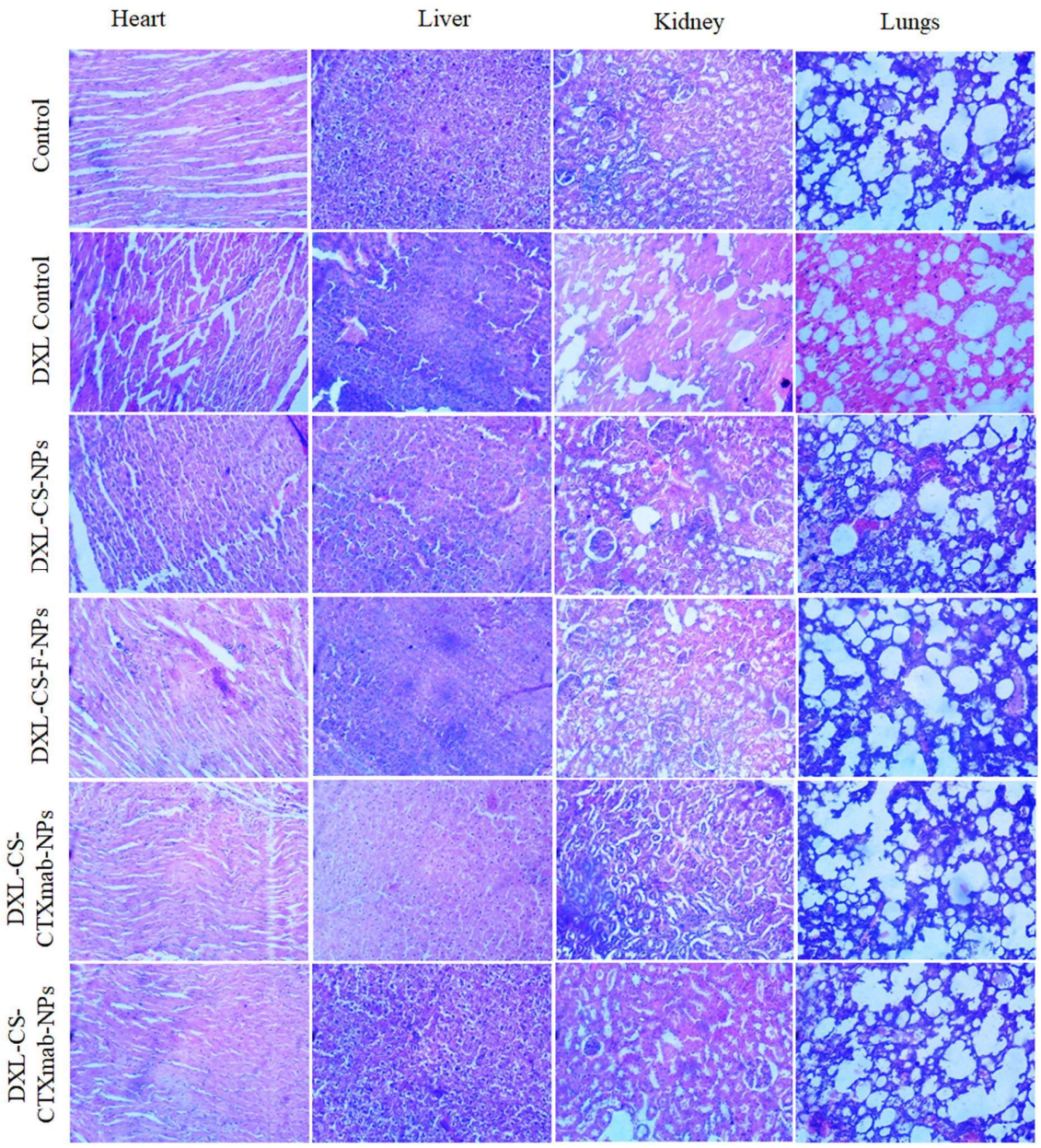

Figure 3.16. Histopathological assessment of the heart, liver, kidneys and lungs of the Wistar rats treated with A) saline control, B) DXL-CS-NPs, DXL-CS-F-NPs, DXL-CS-CTXmab-NPs and DXL-CS-F-CTXmab-NPs

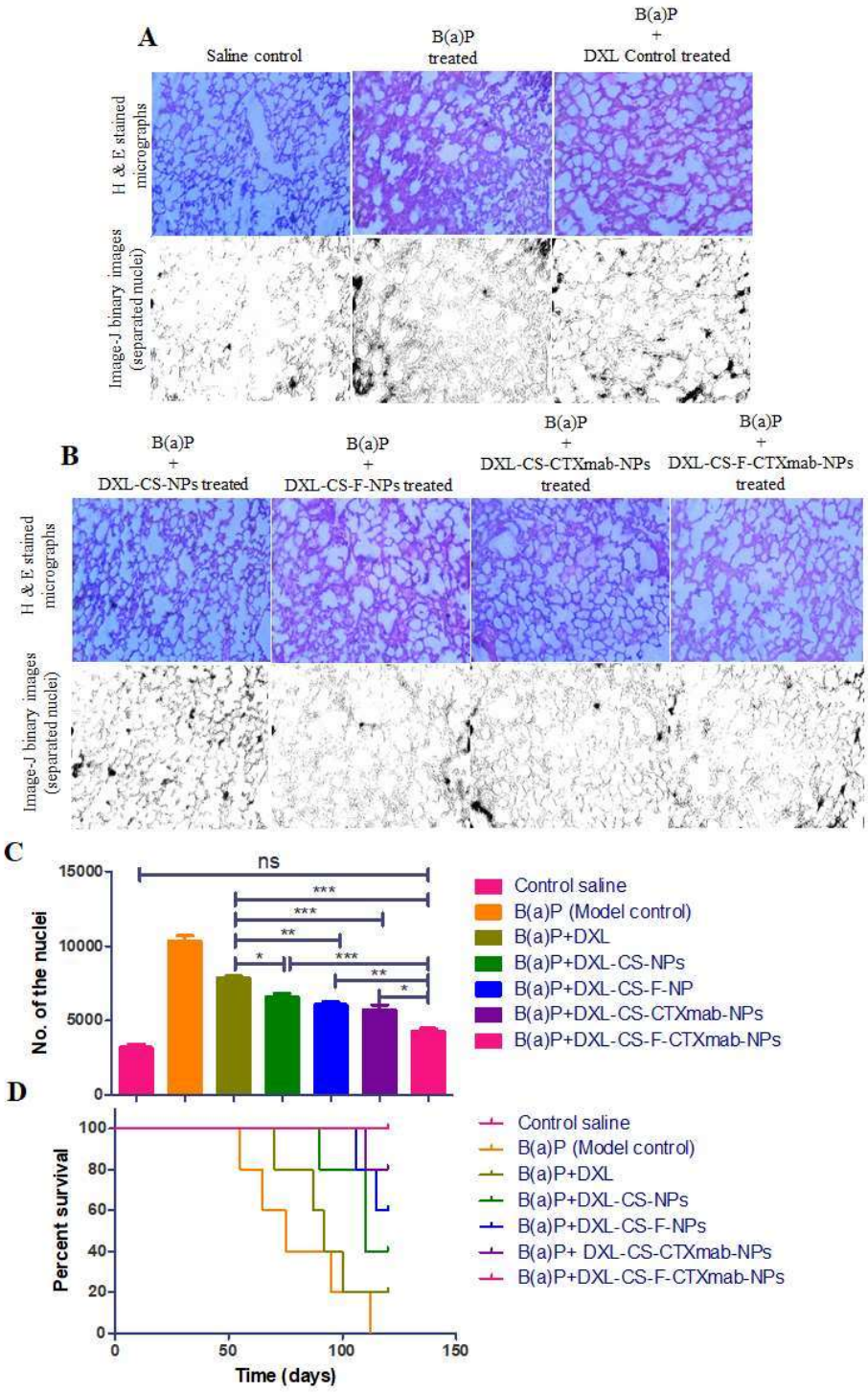

Figure 3.17. HE-stained micrograph and image-J processed binary B and W images of the separated blue channels of A) saline control, cancer model control, and DXL control-treated mice; B) DXL-CS-NPs, DXL-CS-F-NPs, DXL-CS-CTXmab-NPs and DXL-CS-F-CTXmab-NPs. C) Number of the nucleus determined by analyzing the corresponding B and W images of respective animal groups and D) Kaplan-Meier survival analysis of the corresponding groups of the mice up to 120 days

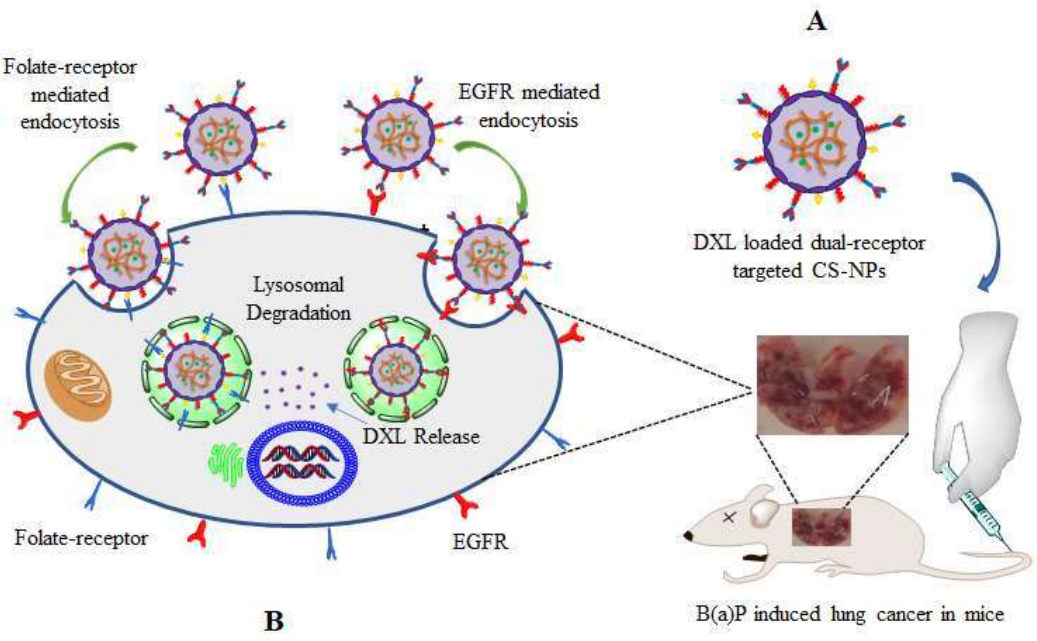

Figure 3.18. Diagrammatical representation of (A) i.v. administration of the DXL loaded dual-receptor targeted CS-NPs in B(a)P induced lung cancer mice and; (B) their cellular uptake mechanism

3.6. Conclusion

In this study, we developed dual-receptor targeted CS-NPs for effective lung cancer therapy. The dual-receptor targeted CS-NPs were prepared to achieve both the strategies of active targeting e.g., pre-conjugation for folic acid targeting and post-conjugation for cetuximab targeting (**Figure 3.18)**. Prepared formulations were screened for physicochemical parameters by DLS, SEM, TEM, AFM. Also, surface chemistry, *in-vitro* release, cellular uptake and cytotoxicity studies were performed. The size, PI and surface charge values were acceptable. The presence of folic acid and cetuximab on the surface of CS-NPs was confirmed by the XPS survey. The entrapment efficiency of targeted (single and dual-ligand decorated) nanoparticles was slightly lesser than non-targeted nanoparticles. The *in-vitro* drug release was found to be slow and sustained at pH 7.4. Whereas, it showed initial burst release at pH 5.5. From comparative cytotoxicity study

on A-549 cells, The IC_{50} value of dual-receptor targeted nanoparticles was found to be 34 times less than that of DXL control. C6 loaded dual ligand decorated CS-NPs showed the highest area of the green channels (10.2 %) as compared to pure C6 (3.6 %), non-targeted (5.6 %), folate targeted (6 %), cetuximab targeted (6.7 %) CS-NPs during uptake studies. Pharmacokinetic evaluation of nanoparticles was performed in Wistar rats which showed improved relative bioavailability, half-life and mean residence time in comparison with the DXL control. The improved half-life of CS-NPs is also establishing its very role in achieving longer-circulation and sustained release of DXL. The anticancer efficacy of the DXL loaded formulation was determined on the B(a)P induced lung cancer mice model, by analyzing the total number of nuclei of the HE-stained microscopic slides of each treatment group. As a result, when compared to other formulations, the dual-targeted chitosan nanomedicine showed the highest anticancer activity and prolonged survival rate. Whereas, it improved the pharmacokinetics of DXL and exhibited better safety on Wistar rats. Hence, the outcomes of the proposed study have been proved to be adequate with a dual receptor targeting approach for advanced lung cancer treatment.